Review Article : Atomic layer deposition of optoelectronic materials

Leskelä, Markku

2019-05

Leskelä , M , Mattinen , M & Ritala , M 2019 , ' Review Article : Atomic layer deposition of optoelectronic materials ' , Journal of Vacuum Science and Technology. Part B. Microelectronics and Nanometer Structures , vol. 37 , no. 3 , 030801 . https://doi.org/10.1116/1.5083692

http://hdl.handle.net/10138/306889
https://doi.org/10.1116/1.5083692

Review Article: Atomic layer deposition of optoelectronic materials

Markku Leskelä, Miika Mattinen, and Mikko Ritala

Citation: Journal of Vacuum Science & Technology B **37**, 030801 (2019); doi: 10.1116/1.5083692
View online: https://doi.org/10.1116/1.5083692
View Table of Contents: https://avs.scitation.org/toc/jvb/37/3
Published by the American Vacuum Society

Review Article: Atomic layer deposition of optoelectronic materials

Markku Leskelä,[a] Miika Mattinen, and Mikko Ritala
Department of Chemistry, University of Helsinki, PO Box 55, FI-00014 Helsinki, Finland

(Received 30 November 2018; accepted 18 March 2019; published 5 April 2019)

Optoelectronic materials can source, detect, and control light wavelengths ranging from gamma and x rays to ultraviolet, visible, and infrared regions. Optoelectronic devices are usually systems that transduce electricity to optical signal or vice versa. Optoelectronic devices include many modern necessities such as lamps, displays, lasers, solar cells, and various photodetectors. Some important research topics in the field of optoelectronics materials are development of new materials, new technologies for fabricating materials, and design of device structures. Atomic layer deposition (ALD) is a technology that was developed in the early 1970s for manufacturing high-quality luminescent and dielectric films to be used in AC-driven thin film electroluminescent (TFEL) displays. Monochromic yellow-black displays based on a ZnS:Mn luminescent layer have been manufactured industrially using ALD since the mid-1980s. Multicolor displays (green-yellow-red) were successfully realized by filtering the broad emission band of ZnS:Mn or adding another luminescent material, e.g., green-emitting ZnS:Tb or SrS:Ce. However, applicable full-color AC TFEL devices could not be developed because of the lack of an efficient deep blue-emitting phosphor. Currently, the most promising application area in TFEL displays is transparent displays, which are commonly used in various vehicles. In the mid-1980s, epitaxial III-V semiconductors were studied using ALD. It was shown that manufacturing real epitaxial [atomic layer epitaxy (ALE)] films is possible for different III (Al, Ga, In) and V (N, P, As) materials. The advantages of ALE processing compared to more traditional metalorganic chemical vapor deposition or molecular beam epitaxy methods have remained low, however, and ALE is not used on a large scale. Research continues to be carried out using ALE, especially with nitride films. Thin film solar cells have continuously received attention in ALD research. ALD films may be used as both an absorber (CdTe, SnS) and a passivation [In_2S_3, Zn(O,S)] material. However, in the solar cell field, the real industrial-level use is in passivation of silicon cells. Thin ALD Al_2O_3 film effectively passivates all types of silicon cells and improves their efficiency. Transition metal dichalcogenides are emerging 2D materials that have potential uses as channel materials in field-effect transistors, as well as phototransistors and other optoelectronic devices. The problem with achieving large-scale use of these 2D materials is the lack of a scalable, low-temperature process for fabricating high-quality, large-area films. ALD is proposed as a solution for these limitations. This review covers all of these ALD applications in detail.
https://doi.org/10.1116/1.5083692

I. INTRODUCTION

This review highlights selected optoelectronic applications where thin films made by atomic layer deposition (ALD) are used. Historically, the most interesting application of ALD has been the thin film electroluminescent (TFEL) flat-panel display. The TFEL was the goal when Suntola started the development of a new deposition technology in the early 1970s.[1,2] TFEL displays were theoretically possible at that time, but AC-driven devices could not be realized because of the low quality of thin film materials. AC-driven thin film electroluminescent (ACTFEL) devices use high voltages (>100 V) that lead to high electric fields (>1 MV/cm).[3] The ALD method—called at that time atomic layer epitaxy (ALE)—was developed for the production of thin films for ACTFEL devices. ALD is a chemical gas-phase technique. The characteristic feature distinguishing ALD from CVD is the alternate supply of precursors one at a time on the substrate. Also, in ALD, the reactor is purged after each of the reactant pulses. The process conditions are adjusted so that all the surface reactions are saturative and purge steps complete. This allows the film growth to be self-limiting, ensuring uniform films over large and complex-shaped substrates.[4] Pulsing and purging steps leading to layer-by-layer growth of films make the ALD method slow. However, in many of the optoelectronic applications, the slow pace of ALD can be mitigated by using large batches of substrates or so-called spatial ALD.[5]

In the mid-1980s, ALE research interests shifted to growth of epitaxy of III-V semiconductors with obvious applications for light-emitting diodes and semiconductor lasers.[6,7] Intensive research on III-V semiconductors lasted

Note: This paper is part of the Special Topic Collection Honoring Paul Holloway for Contributions in Luminescent Materials Growth, Synthesis and Characterization.
[a]Electronic mail: markku.leskela@helsinki.fi

over a decade before declining. However, interest in the field resurged in the 2010s with a focus on plasma-enhanced ALD of nitride films.[8]

Different types of solar cells can benefit from ALD when it is used for the deposition of both passive and active layers. In silicon solar cells, ALD oxide passivation layers can improve performance.[9] ALD films can be applied for several purposes in dye-sensitized solar cells (DSSC) and perovskite cells, with passivation and encapsulation being the most studied properties. Thin ALD oxide films can improve the aging properties of the cells.[10,11] In thin film solar cells, both absorber and passivation materials have been deposited by ALD, but large-scale breakthroughs have yet to be achieved.[12]

Conformal pinhole-free ALD films are excellent not only in passivation but also in the encapsulation of optoelectronic devices, organic light-emitting diodes (OLED) displays being one example. A 30–50 nm thick ALD Al_2O_3 film encapsulates the OLED very well extending the lifetime of the device to thousands of hours. Even better results can be achieved with Al_2O_3/ZrO_2 nanolaminates.[13,14] OLED encapsulation is one of the growing fields of ALD application. Inorganic phosphor materials—especially sulfides used in LEDs—are also sensitive in ambient conditions and may be protected by ALD oxides.[15,16]

Two-dimensional transition metal dichalcogenides (TMDC) have strong molecular intralayer bonds but weak interlayer bonds, giving rise to layered structures and anisotropic properties. Depending on the metal and chalcogen, the materials can be insulators, semiconductors, semimetals, or metals in nature. Interestingly, the properties can change when going from bulk to one or a few monolayers (MLs).[17] MoS_2 has been one of the most studied TMDC materials. When thinned to a monolayer, it exhibits a direct bandgap and very promising optoelectronic properties. Using ALD for TMDCs is a very new application, but several processes have already been developed for MoS_2 and other TMDCs.[18,19] More work is still needed in the development of ALD processes for TMDCs, in particular, on new materials, such as metallic TMDCs, as well as on the improvement of crystallinity and grain size. For most applications, TMDCs are used in ultrathin form but need to be deposited on large areas. Both of these factors support the use of ALD for optoelectronic applications, such as photodetectors and photovoltaics.

II. ELECTROLUMINESCENT DISPLAYS

The inorganic (ACTFEL device has a so-called double insulated metal-insulator-semiconductor-insulator-metal structure where the light-emitting layer is sandwiched between dielectric layers and electrodes. The electrodes have typically been transparent conductors and metals and their order can be traditional (transparent electrode on glass—viewing through glass) (Fig. 1) or inverted (metal electrode on glass and transparent electrode as front electrode—viewing through transparent electrode).[20] In modern transparent displays, both electrodes are transparent.[21] ACTFEL display takes advantage of the all-solid structure, and therefore it tolerates harsh conditions such as low and high temperatures, vibrations, and heavy dust. In addition, its brightness is high, viewing angle is wide, and lifetime is long. In the 1990s, it was said that ACTFEL was the most reliable display technology on the market.[22] Other flat-panel display techniques, however, have quickly developed since the 1980s and 1990s and TFEL devices now have a very small market share with a focus only on niche applications. The key disadvantages of ACTFEL displays include high voltage (high power) requirements and lack of full-color displays. Multicolor displays are available, but the lack of a deep blue-emitting phosphor has prevented the realization of full-color devices.[23]

ACTFEL devices were the inspiration for the development of the ALD (ALE) method. A great amount of research in the 1980s was focused on ALD, as well as other techniques for depositing thin film inorganic films for electroluminescent (EL) displays. Yellow-emitting monochromatic displays based on ZnS:Mn was the research focus, and commercial display production based upon this material was begun in the mid-1980s (Fig. 2).[24] One of the main benefits of the ALD technique was the capability to grow high-quality, dense dielectric oxide films. High dielectric strength (>1 MV/cm) is required from the insulators. Another benefit of ALD is the possibility to grow the dielectric-phosphor-dielectric stack in one process. It is notable that the layers are thick (dielectrics 200 nm and luminescent film 0.5–1 μm). ALD is a slow process due to the layer-by-layer growth mode but the use of large batches of substrates in one process makes it cost competitive.[21] The possibility to make the whole dielectric-luminescent-dielectric layer in a continuous process and superior quality of ALD films also favor ALD over other thin film technologies. However, ACTFEL displays are the only thick-film application of ALD and in microelectronics and passivation and protection applications, ALD films are usually 1–100 nm thick.

The dielectric oxides studied for EL displays included binary oxides such as Al_2O_3 and Ta_2O_5.[25,26] It was quickly noted that nanolaminates of two oxides give superior properties compared to binary oxides.[24] Later, it was shown that nanolaminates were also applicable for tuning electrical and chemical properties of oxide films.[27–29] Amorphous Al_2O_3 nanolaminated with crystalline TiO_2 (ATO) is the dielectric material used in commercial EL devices today. Both Al and Ti oxides were made from chlorides and water. It is useful to understand the possible interface problems encountered during interface modulation. $AlCl_3$ etches the deposited TiO_2 film, but the etching process is effective only during the first few $AlCl_3$ cycles and reaches only to 1 nm depth.[30,31] The most common ALD aluminum oxide process utilizes trimethyl aluminum (TMA) and water.[32] It is considered to be the best available ALD process. However, in making ATO, TMA reduces titanium to +3, which gives the film a dark color and weakens the dielectric properties. This is not acceptable in EL devices. With proper process parameters, the darkening effect can be minimized. If alkaline earth sulfides (CaS, SrS) are used as the luminescent layer, other problems appear in the deposition

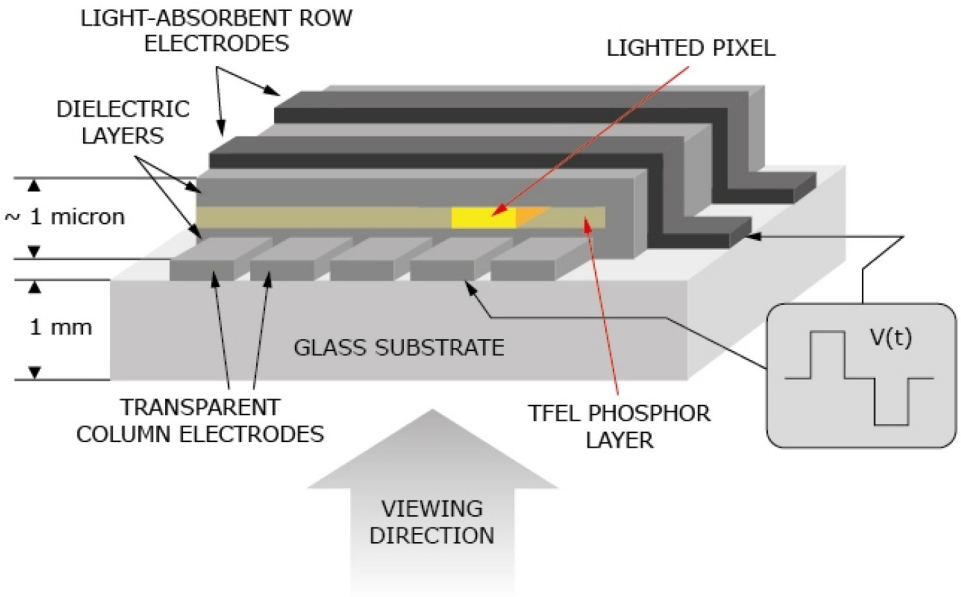

FIG. 1. Cross section of an ACTFEL device with conventional structure. (Figure courtesy of Beneq, www.beneq.com.)

of dielectric oxides. Aluminum chloride is not a good choice for a precursor, as stable $CaCl_2$ or $SrCl_2$ can form. Water vapor is not favorable for the alkaline earth sulfides, but it seems that the TMA water process does not significantly damage the luminescent film.[33] There are alternative precursors for aluminum oxide, viz., different aluminum alkoxides, alkohols as oxygen source, and nonwater containing processes using metal alkoxide and chlorides.[34,35] Chloride-free processes are applicable in connection to alkaline earth sulfide films, whereas etching is less effective with the water-free processes compared to the original chloride-water process.

The physical vapor deposition (PVD) methods, sputtering and evaporation, have been the most commonly used deposition methods of ZnS:Mn-based yellow luminescent layers for ACTFEL displays on a research scale.[36,37] Also, in the later studied alkaline earth sulfide and ternary thiogallate luminescent films, PVD methods were dominant.[38] In industrial display manufacturing, however, ALD is dominant. ZnS:Mn films are produced with metal chlorides and H_2S. The deposition temperature is 500 °C, and the Zn and especially Mn chloride require high source temperatures.[39] Lower deposition temperatures can be used with Zn acetate[40] and dimethyl[41] or diethyl zinc.[42] In these cases, the Mn doping also requires metal organic precursors.[43] By using metal organic precursors, potential chlorine residues can be avoided. Chlorine can be harmful and cause aging of the devices. Growth temperature has an effect on the crystal structure of ZnS, viz., hexagonal phase is formed at high temperatures (>400 °C) and cubic phase at low temperatures (<400 °C).[44] This has been studied thoroughly for zinc chloride and zinc acetate processes.[45,46] Growth rates in the chloride and alkyl zinc processes are very similar, about 1 Å per cycle, whereas in the acetate process, the rate is significantly higher at 2.6 Å/cycle. This is attributed to the formation of a volatile tetramer $[Zn_4O(OAc)_6]$ in the gas phase that adsorbs on the surface.[47] The two crystalline phases of ZnS have different bandgaps: hexagonal 3.8 and cubic 3.7 eV. The

FIG. 2. Yellow-emitting ZnS:Mn EL displays: traditional and transparent forms. (Photos courtesy of Beneq, www.beneq.com.)

bandgap has an effect on the broad luminescence band of manganese, the difference in the maximum wavelength being about 5 nm at the emission maximum (580 and 585 nm in hexagonal and cubic structures, respectively).[48] The color difference is noticeable with the naked eye. The optimum Mn concentration in the electroluminescent ZnS films is about 0.8–1 mol. %. The emission intensity and weakly dependent on the concentration because of the forbidden nature of the Mn electronic transition. However, the intensity decreases at higher concentrations due to concentration quenching. The emission color is red shifted along with higher concentration. At the optimum concentration, the emission spectrum of Mn is a broad band from 520 to 640 nm, peaking at yellow.

The most important characteristics of EL devices are luminance (L versus V), luminous efficiency (η versus V), and transferred charge (ΔQ versus V) (Fig. 3). All curves in the figure show a threshold voltage above which the luminescent layer loses its insulating properties and electrons from the insulator–luminescent layer interface are injected into the luminescent layer and excite the Mn dopant ions. In the case of ZnS:Mn, an electric field of the order of 2×10^6 V/cm is needed.[49] In displays, a steep L-V curve is preferred, which enables the modulation of the on-off state with a small voltage change. Efficiency of the luminescence is very important and in practice values higher than 1 lm/W are needed.[50] Luminance values are usually reported in the application conditions, viz., at a voltage 40 V above the threshold voltage and 60 Hz frequency. ALD-fabricated ZnS:Mn devices fulfill the requirements and show an average luminance of 300 cd/m^2 and efficiency of 5 lm/W.

The increasing thickness of the ZnS:Mn film increases both the EL luminance and efficiency. Thus, relatively thick (>500 nm) films are used in practice.[51] Luminescence generally depends on the crystallinity of the host material—the better crystallinity, the higher the luminescence, as defects in the material act as killer centers for light emission. ALD-grown ZnS:Mn shows columnar structure and larger grains than films made by PVD methods.[52] Close to the interface, the luminescent layer is not as crystalline as in the bulk of the film. In addition, this layer does not show luminescence and so is called a "dead layer," which in the ALD films is about 35 nm thick.[51,53]

One of the benefits of ACTFEL displays is their long life that can extend to tens of thousands of hours. However, ACTFEL displays show aging that is seen as a shift in the L-V curve. Depending on the fabrication method, the devices may show an increase (CVD) or decrease (ALD) of the threshold voltage following accelerated aging of 1000 h.[23,54] In addition to the threshold voltage shift, the steepness of the L-V curve may soften. In practice, the displays are aged prior to use.

Monochrome EL displays have been produced by ALD consistently since the mid-1980s. These displays have a clear niche market where their favorable properties such as brightness, wide viewing angle, ruggedness, and wide operation temperature range are appreciated. Displays for different vehicles and industrial and hospital instruments require these properties. The development of transparent displays further widens the applications in vehicles enabling interactive displays in windshields, side windows, sun-roofs, and doors.

Color displays can be divided into two groups: multicolor and full-color displays. Multicolor displays show two or more colors while full-color devices can show an infinite number of colors. Full-color displays contain blue, green, and red phosphors and the triangle they form in the color coordinate gamut determines the colors they can produce. Full-color displays can produce pure white light and for commercial displays, the areal white luminance requirement is 50 cd/m^2 at 60 Hz. For different color pixels, this means luminance requirements of 15.4, 131.6, and 53 cd/m^2 for blue, green, and red pixels, respectively.[55]

Requirements for EL phosphors are host material must have a large enough bandgap to enable emission of visible light from the dopant ions; the material must behave as insulator before reaching the luminescence threshold voltage; the film material must withstand high electric fields; a suitable dopant ion must be available to give bright emission with desired color and a good fit to the lattice of the host material; must be tolerant to high temperatures; and finally, there must be a deposition method for the production of high-quality

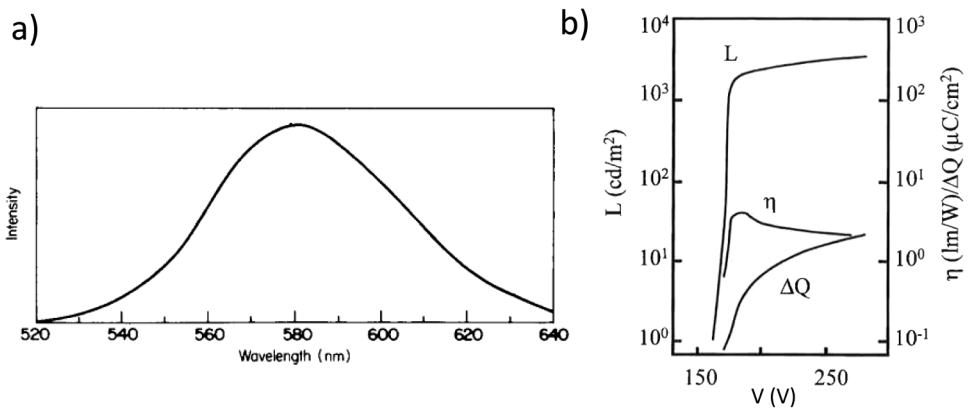

FIG. 3. Typical (a) EL emission spectrum and (b) luminance-voltage (L-V), efficiency-voltage (η-V), and transferred charge-voltage (ΔQ-V) curves of a ZnS:Mn EL device. Intensity in (a) given in arbitrary units. Reprinted with permission from Leskelä *et al.*, "Semiconductors and semimetals," in *Electroluminescence II*, edited by G. O. Müller (Academic, New York, 1999), Vol. 65, p.107. Copyright 1999, Elsevier.

film. Materials that best fulfill the requirements are II-VI compounds (ZnS, CaS, SrS, ZnSe), some ternary chalcogenides and oxides. Ternary compounds often suffer from bandgaps that are too low and oxides ones that are too high. Excitation of the dopant ions occurs in electroluminescence via electron impact excitation and the dopant should have a large cross section for that process. In addition, the excited state of the dopant ion should lead to efficient emission and low nonradiative losses. Manganese and rare earth ions best fit these requirements.

Because the high energy portion of the broad emission band of ZnS:Mn is in the red region, a Cd(S,Se) filter can be used to obtain red emission, in terms of color coordinates that are closest to the cathode ray tube standard.[56] In fact, filtered ZnS:Mn is currently the brightest (75 cd/m^2) and most efficient (0.8 lm/W) red ACTFEL phosphor. Values of 60 Hz and 35 V above the threshold voltage were recorded.[50] ZnS:Mn is ready for commercial applications even for full-color displays. The green emission obtained by filtering from ZnS:Mn gives good luminance (80 cd/m^2) with color coordinates $x = 0.45$ and $y = 0.55$ [resulting in a yellow hue (Fig. 4)]. Achieving a deeper green requires a different filter but results in lower luminance.

Lanthanide ions are known dopants that produce different colors. They are widely used in different phosphor materials applied for lighting. The most commonly used ions are terbium (green), europium (red), cerium (blue-green), samarium (red), and thulium (blue). These all have been studied as dopants in ZnS thin films, and their electroluminescent properties have been characterized.[23,50,55] Tb^{3+}, Eu^{3+}, Sm^{3+}, and Tm^{3+} ions show similar emission spectra independent of the matrix (i.e., chemical environment) in which they are located. This is because of the 4*f*-4*f* electronic transition. Both luminance and efficiency in Sm- and Tm-doped ZnS remain low and these materials cannot be considered potential phosphors for color EL devices. The luminescence of terbium in ZnS is typically green with the main emission lines located at 540–550 nm (Fig. 5). The luminance and efficiency in ALD processed films typically show values of 70 cd/cm^2 and 0.6 lm/W. The Tb^{3+} ion is much larger than Zn^{2+}, and the substitution of Zn in the lattice is limited. In addition, there is an oxidation state mismatch. Intentional addition of a codopant such as F^- or O^{2-} results in more efficient luminescence. Yoshino *et al.*[58] have reported luminance values of 100–120 cd/m^2 for PVD ZnS:TbOF films and efficiencies of 1.3–1.7 lm/W. When terbium was introduced in ALD ZnS thin films, a β-diketone thd (2,2,6,6-tetramethyl-3.5-heptanedione) complex was used as the volatile precursor. When $Tb(thd)_3$ terbium is coordinated to oxygen, it seems that at least a part of the oxygen remains on the surroundings Tb in the ZnS lattice. The coordination resembles that in oxysulfide, which was shown to be beneficial for electroluminescence.[59,60] The color coordinates of ZnS:Tb, $x = 0.30$, $y = 0.60$, are better, and the hue is greener than that of filtered ZnS:Mn. Also, the efficiency and luminance of ZnS:TbOF are close to those required for commercial products.

The rare earth ions are large and they fit better as dopants into alkaline earth containing matrices than in ZnS. Therefore, alkaline earth sulfides (CaS, SrS, BaS) and thiogallates ($SrGa_2S_4$) have been studied as matrix materials for EL phosphors. In ALD processing, the problem was to find suitable volatile, thermally stable precursors. Large ions with low charge form a challenge since coordination saturation is difficult to achieve due to consequential thermal instability or oligomerization of the complex. Oligomerization results in high molar mass, which reduces the volatility. The challenge

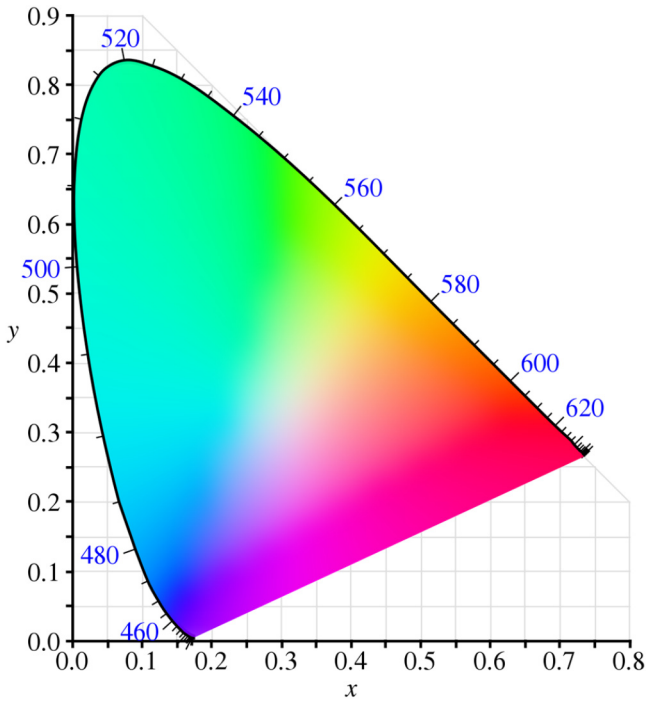

FIG. 4. CIE 1931 color coordinate diagram (Wikimedia Commons, https://commons.wikimedia.org/wiki/File:CIE1931xy_blank.svg).

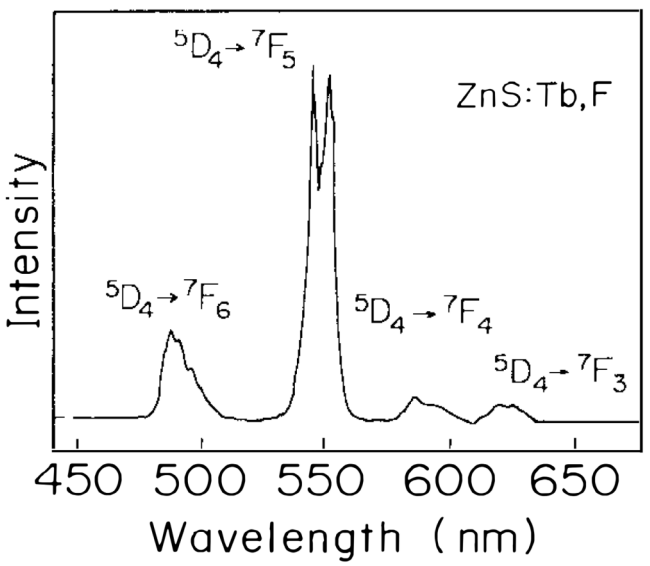

FIG. 5. EL spectrum of ZnS:Tb,F thin film made by PVD (Ref. 57). Reprinted with permission from Ohnishi, Annu. Rev. Mater. Sci. **19**, 83–101 (1989). Copyright 1989, Annual Reviews, Inc.

is very similar for alkaline earth and rare earth metals. β-diketonates were the first widely used volatile complexes for all these metals.[61] Later, many new volatile precursors, such as cyclopentadienyl, alkylamide, and amidinate complexes, were developed.[62] β-diketonates react well with H_2S in ALD but oxide compounds cannot be prepared from them and water. Cyclopentadienyl compounds react with both water and ozone to form oxide films and hydrogen sulfide to form sulfide films.[63]

Electronic transitions in Ce^{3+} and Eu^{2+} ions occur between 5*d* and 4*f* orbitals and the energy of this transition depends on the chemical environment. Depending on the host material, these ions may emit light from UV wavelengths to red. In alkaline earth sulfides, Eu^{2+} shows red and Ce^{3+} shows blue-green emission. Strontium sulfide doped with cerium was extensively studied as a possible blue phosphor for full-color EL devices since the first report in 1984.[64] ALD processing of the devices used thd-precursors.[65] The EL properties of the SrS:Ce devices are promising, with luminance at 100 cd/m^2 and efficiency in the range of 0.8–1.6 lm/w. However, the emission color appears too green, the main peak located at 485–490 nm with a shoulder at 540–560 nm [color coordinates x = 0.3, y = 0.5 (Fig. 6)].[66,68] Deep blue emission can be filtered from SrS:Ce, but then 90% of the luminance is lost. Many methods have been studied to enhance and blue-shift the emission of Ce in SrS, such as decreasing the Ce concentration, co-doping with alkali or halogen ions, replacing Sr partially with other alkaline earth metals, replacing sulfur partially with selenium, filling vacancies, improving the crystallinity using a flux, and annealing in different atmospheres.[23] Lowering the Ce concentration, replacing some sulfur by selenium or co-doping with fluorine all cause the emission peak to shift 10 nm to lower wavelengths.[38,69–71]

Because of the greenish emission of SrS:Ce, a better blue-emitting phosphor was needed for full-color TFEL displays. Studies to develop a better blue-emitting phosphor had two directions: new dopant ions for SrS or new host material. Cu and Pb are examples of new dopant ions that can produce more blue emission in SrS. The EL spectrum of copper-doped SrS films consists of a broadband peaking at 480 nm. Even better blue material is obtained by co-doping the film with silver, for which the emission peak is shifted to 430–440 nm.[72] The films studied were fabricated mainly by PVD techniques, due to the limited availability of acceptible copper and silver ALD precursors at that time. For SrS:Cu, Ag deep blue emission (x = 0.17, y = 0.13) was recorded with luminance of 20 cd/m^2 and efficiency of 0.15 lm/W. However, these values are still not sufficient for commercial products. Lead doping was possible with ALD in the 1990s.[73] The use of CaS instead of SrS as a matrix gave better results and blue EL (x = 0.15, y = 0.15) with luminance of 80 cd/m^2 was reported.[74]

Ternary sulfides have proven to be possible matrix materials for blue-emitting phosphors with the most studied being thiogallates, such as $CaGa_2S_4$ and $SrGa_2S_4$. Cerium yields the desired blue emission color in thiogallates but the luminance and efficiency remain low.[23,75] ALD processing of thiogallates is challenging and the data reported in the literature are based on PVD-deposited films.

Filtered ZnS:Mn gives quite good red EL properties but efforts were focused on finding a material exhibiting more saturated red emission. The EL spectrum of CaS:Eu^{2+} is a very broad band between 600 and 700 nm (color coordinates x = 0.68, y = 0.31),[68,76] but the luminance and efficiency are low. ZnS:Sm shows similar luminance and efficiency numbers as CaS:Eu but with less deep red color.

One approach to make full-color TFEL displays has been via white light. It is possible to get all colors by filtering from white light. White EL can be obtained by three ways: single doping of ZnS, double doping of SrS, or by stacked layers of two materials. The last approach has produced the best results and prototype ZnS:Mn/SrS:Ce stacked layers can produce 470 cd/m^2 with 60 Hz frequency, but the deep blue colors are still missing making the white light yellowish.

Full-color EL display research did not result in industrial products and only multicolor displays could be developed to the application level. Reasons for the unsuccessful outcome were problems in finding efficient deep blue phosphor material and fast development of the competing thin film display

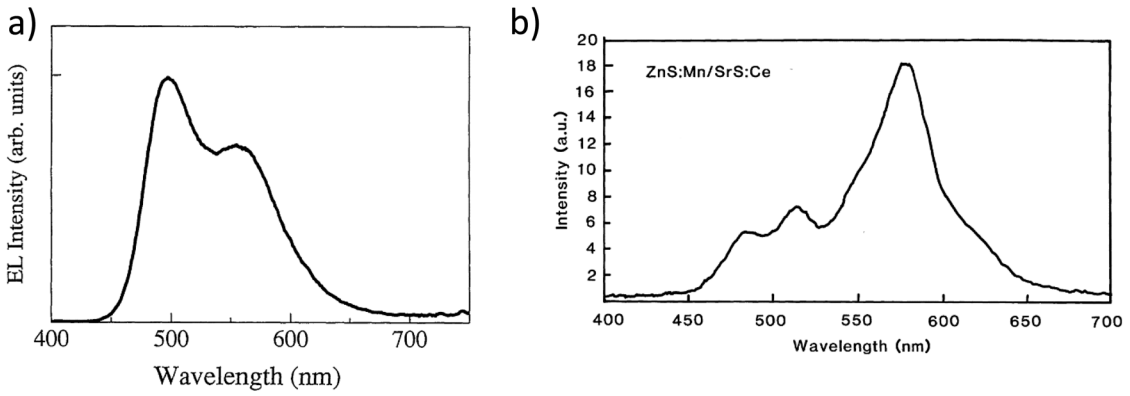

FIG. 6. (a) EL spectra of SrS:Ce and (b) ZnS:Mn/SrS:CeTFEL devices (Refs. 66 and 67). The device in (b) has been prepared by PVD. (a) Reprinted with permission from Leskelä, Alloys Compd. **275–277**, 702 (1998). Copyright 1998, Elsevier. (b) Reprinted with permission from Inoue *et al.*, Jpn. J. Appl. Phys. **36**, 4335 (1997). Copyright 1997, The Japan Society of Applied Physics.

technologies such as liquid crystal displays and OLED. The intense research on full-color EL displays, however, resulted in many new ALD processes for new elements, such as alkaline earth metals, rare earth metals, gallium, copper, silver, and lead. The precursor chemistry of these elements has later been utilized for many applications, for example, in high dielectric constant oxide and metal films in microelectronics.

III. EPITAXIAL COMPOUND SEMICONDUCTORS

ALD was originally called atomic layer epitaxy, so it is understandable that the method received attention from semiconductor researchers who traditionally have had a greater need for epitaxial films. The principle of ALE was first proven in a molecular beam epitaxy (MBE) reactor for the deposition of ZnTe from the elements and ZnS from zinc chloride and hydrogen sulfide.[77,78] Later, Pessa's research team studied epitaxial CdTe films grown from elements.[79,80] The research is summarized in a review paper.[81] Yao and his team focused their studies on zinc chalcogenides and studied the ALE on gallium arsenide.[82] The ZnSe-ZnTe system was further studied, and it was shown that the ALE-strained superlattices have superior optical properties when compared to MBE-made samples.[83]

The studies on II-VI ALE continued during the 1990s in a few groups. In the following, a few examples are mentioned. Faschinger *et al.* studied many zinc and cadmium chalcogenide processes using elements as precursors and verified the saturative growth rate in the case of tellurides to be 0.5 monolayer per cycle.[84] They also made superlattices from different materials and noticed that efficient photoluminescence is obtained from short-period superlattices, whereas for longer period superlattices, the luminescence drops drastically.[85] Hsu grew ZnS, ZnSe, and ZnS_xSe_{1-x} as well as strained superlattices of ZnS/ZnSe from dimethyl zinc and hydrides. He used silicon substrates, whereas most other II-VI ALE studies focused on GaAs. Self-limiting growth occurred at 150–175 °C. Optical characterization showed good properties for superlattices containing 25 pairs of layers.[86] Hernandez-Calderon *et al.* specifically focused on Zn-Cd selenide superlattices. Three-pair structure showed efficient green emission while a decrease in brightness was observed for thicker structures. Deposition temperature also affected the emission wavelength.[87]

ALE attracted more interest in studies of III-V semiconductors than for the II-VI types. The studies on GaAs started in the mid-1980s and the early studies have been summarized in review papers.[81,88–90] Very different reactors were employed by various groups, including atmospheric pressure MOVPE,[91] UHV-MOMBE,[92] hydride-VPE,[93] and laser-assisted ALE (MOVPE).[94] Precursors used were gallium alkyl compounds TMG, TEG, and similarly for Al and In. AsH_3 was the most common arsenic precursor. Usui and Sunakawa[93] preferred chlorides as gallium precursors (GaCl and DEGaCl). The goal of these studies was to obtain the ideal of one monolayer per cycle growth for the epitaxial films. Saturation of the growth rate per cycle as a function of precursor (TMG and arsine) doses was achieved and the growth proceeded almost 1ML per cycle at reaction temperatures close to 500 °C.[92] The results varied depending on the reactor system used. Relatively high temperatures were needed in the case of the TMG precursor, and the temperature window could be narrow as shown in the case of the MOMBE reactor where the ALE mode was registered at 490–510 °C.[92] Lower deposition temperatures could be achieved with the triethyl gallium precursor[95] or by using laser activation (Fig. 7).[96,97]

ALE processes have been studied for most of the III (Al, Ga, In)–V (N, P, As) compounds using mainly metal alkyl compounds and nonmetal hydrides as precursors. Thermal

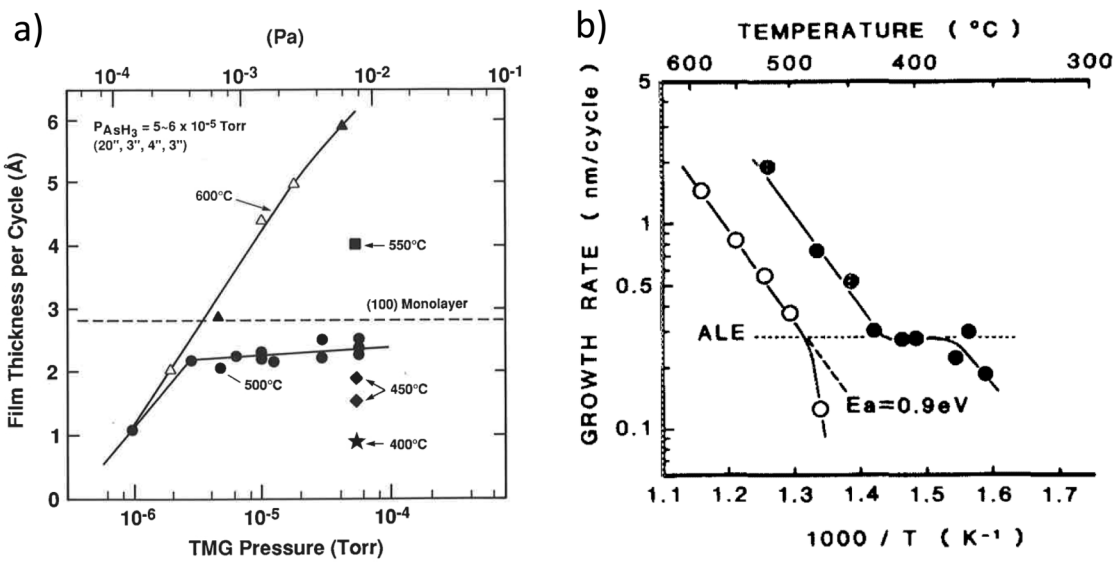

FIG. 7. (a) GaAs film thickness per cycle as function of trimethyl gallium pressure at different temperatures in an MOMBE reactor. Reprinted with permission from Nishizawa *et al.*, J. Electrochem. Soc. **132**, 1197 (1985). Copyright 1985, Electrochemical Society. (b) Growth rate per cycle as a function of temperature for epitaxial GaAs grown without (open circles) and with laser irradiation (solid circles). Reprinted with permission from Doi *et al.*, Appl. Phys. Lett. **49**, 785 (1986). Copyright 1986, AIP Publishing LLC.

stability and reactivity of the precursors vary and accordingly, the deposition temperatures vary between 300 and 500 °C. With proper selection of precursors and deposition conditions, monolayer growth of epitaxial films was achieved for compounds such as AlAs, GaP, InP, and InAs.[89] Next, the processes of binary compounds were combined for different alloys such as (Al,Ga)As and InGaP. Depending on the pulsing sequence, the compositions could be varied.[98,99] Heteroepitaxial growth is more complicated than homoepitaxial growth because of the different surfaces at the interfaces. However, many groups were able to fabricate different heterostructures from the III-V compounds by ALE.[99,100] A strained-layer superlattice of $(GaAs)_m(GaP)_n$ monolayers is an early example fabricated by Ozeki *et al.*[101]

ALE processing of epitaxial III-V semiconductors has many advantages. Monolayer growth can be achieved and films are very homogeneous over large substrate areas. In heteroepitaxial structures, the interfaces between the layers are sharp. Selective growth has been reported in some cases, i.e., no growth was seen on silicon oxide or nitride masks.[92] Side-wall epitaxy is one of the advantages, and Shaw was the first reporting a large growth rate dependence on crystal planes.[102] ALE can show monolayer per cycle growth irrespective of the orientation of the surface,[103] but this is due to temperature dependence (Fig. 8). Isshiki *et al*. showed that it is possible to achieve selective growth of GaAs on its (100) planes while leaving the (111) planes bare. The selective growth was nicely shown in V-grooved structures on GaAs(100) where the sides of the grooves where (111) oriented.[104] One important application of side-wall epitaxy is GaAs tunnel junction formation, which was widely studied as shown by the review.[105]

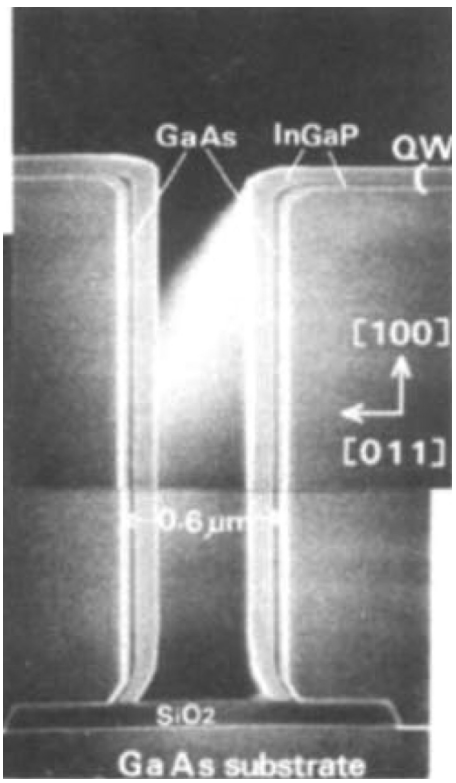

FIG. 8. Cross-sectional SEM image for $In_{1-x}Ga_xP$/GaAs single quantum well structure grown on (011) side walls of a GaAs substrate. Reprinted with permission from Usui *et al*., Appl. Phys. Lett. **56**, 289 (1990). Copyright 1990, AIP Publishing LLC.

Using ALE for III-V compounds poses some challenges. First is the common problem of all ALD/ALE processes, viz., slowness that originates from the pulsing of the precursors. Another problem is the high carbon background in the films, which has a negative impact on the electrical properties. Changing the metal precursor to chlorides helps in lowering the carbon concentration and improved properties have been reported. However, chloride residues may cause other issues.[89] Yet another problem for ALE is the fabrication of III-V alloys and heterostructures since it is difficult to find precursors working at the same temperature. In general, controlling the processes can be challenging due to narrow temperature windows. Improvements have been achieved with plasma or photo assistance. Doping is needed in semiconductors and in ALE, the dopant ions are introduced as layers, called δ-doping. This doping mode is not always the best possible; however, reasonable results have been reported on doping with silicon or selenium.[99]

ALE studies on III-V semiconductors are continuing, with a new focus on ALD of III-V nitrides during the 2010s. Plasma ALD processing is used with the particular aim of lowering deposition temperatures. Processes have been reported for all III-nitrides, including AlN, GaN, and InN as pure materials, doped and mixed, and as nanolaminates. For example, a trimethyl metal precursor $+N_2/H_2$ or NH_3 plasma processing at 200 °C resulted in growth rates of 0.9, 0.3, and 0.6 Å/cycle for AlN, GaN, and InN, respectively.[105,106] The films are polycrystalline and impurity levels are low (C <1%, O 1.5%–2.5%). AlN is the most studied III-V ALD nitride and plasma processing was used in the most reported studies.[8,107–109] The favorable dielectric and piezoelectric properties, thermal conductivity and mechanical rigidity of polycrystalline AlN make them suitable for many industrial applications. GaN and InN are more studied for thin film transistors[110] and metal-semiconductor-metal photodetectors.[111]

Plasma-enhanced ALE has also been employed for the deposition of epitaxial III-V nitride films on sapphire or metalorganic chemical vapor deposition processed III-V surfaces. Processes use a trimethyl metal precursor and N_2 and N_2/H_2 plasma. Binaries and ternaries of AlN, GaN, and InN have been successfully deposited.[112] $Al_xGa_{1-x}N$ ternaries were grown at 350–450 °C, while indium-containing ternaries require lower temperature of 260–300 °C. Quantum well structures have been fabricated and their optical properties characterized.[113,114]

ALE of compound semiconductors was intensively studied from the mid-1980s to mid-1990s. Many papers were published and many things were learned from the surface chemistry between alkyl metal compounds and hydrides of elements in Groups 15 and 16. The studies were often focused on growth mechanisms and conditions conducive for achieving one monolayer growth per cycle. However, the problems associated with ALE (slowness, carbon impurities,

and difficulties with depositing heterostructures at a single temperature) made it unsuitable for large-scale fabrication of devices requiring epitaxial films. Current investigations into nitride films are still in the basic research stages.

IV. SOLAR CELLS

ALD can be applied to photovoltaics (PV) in many ways as can be seen from the recent review papers by Bent and co-workers,[115,116] Niu *et al.*,[117] and Meng *et al.*[118] Here, the topic is only briefly touched upon, giving emphasis to thin film solar cells, and passivation layers used in silicon, dye-sensitized, and perovskite solar cells. The review papers mentioned above also describe the use of ALD passivation layers in quantum dot and colloidal quantum dot sensitized solar cells as well as organic solar cells.

A. Thin film solar cells

Thin film solar cells have been studied and used as alternatives to silicon cells. The thin film PV cells contain several functional thin films that may be prepared using ALD, including absorber, transparent conductor, buffer, and window layers. As early as the late 1980s, ALD thin film research was focused on photovoltaics. CdTe films were grown, first in UHV MBE-type reactors and later in flow-type reactors using elements as precursors. Efficiencies of 14% were reported for cells which were annealed with $CdCl_2$ and had a CdS buffer layer (Fig. 9).[119,120] The buffer layer was also made by ALD using $CdCl_2$ and H_2S. Different transparent conductor oxides (TCO) were also studied at that time, with a focus on applications in PV and electroluminescent displays. Al-doped ZnO was studied in CIS (copper indium selenide) cells while indium oxides and ITO were only characterized as single materials.[121–123] The early ALD studies also included a process for depositing an In_2S_3 buffer layer.[124] ALD processes have been extensively developed to cover different TCOs to be applied in all kinds of optoelectronic applications, as can be seen from a recent review on ALD ZnO.[125] Spatial atmospheric ALD needed in high throughput production has also been exploited for ZnO and ZnO:Al TCOs with good results.[126,127]

The later ALD research on absorbers for thin film solar cells has been basic and focused on selected materials, such as Cu_2S, CIS, and SnS. No breakthroughs have been made and the reported efficiencies are in the range of 2%–6%, much less than that reported for CdTe.[115] Recently, SnS has received attention because of its many promising properties such as high absorption coefficient and good hole mobility. The best films have been processed using pulsed CVD and have had all buffer layers [Zn(O,S), ZnO] made by ALD. Despite many studies on tuning the material and interface properties (H_2S annealing, SnO_2 passivation, Na doping), the highest demonstrated efficiency remains at 4.36%.[128]

The thin film solar cells rely on a pn-junction. The buffer layer is usually an n-type material with a higher bandgap than the p-type absorber. The buffer layer has several roles

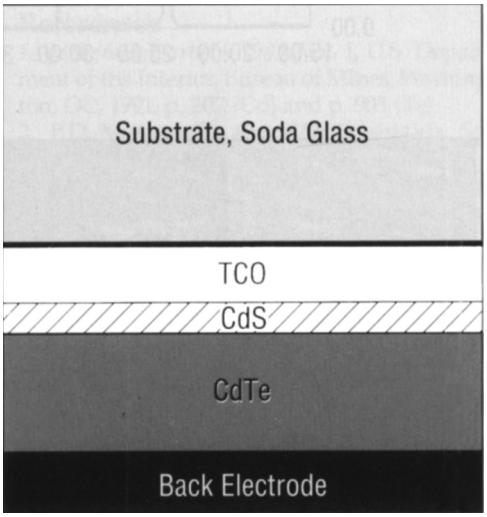

FIG. 9. Cross section of a CdTe thin film solar cell. Reprinted with permission from Suntola, MRS Bull. **18**, 45 (1993). Copyright 1993, Cambridge University Press.

in band alignment, including increasing the depletion layer (increasing open-circuit voltage) and protection of the absorber. Chemical bath deposited CdS film is the most applied buffer layer, but several ALD materials have been studied, including ZnS, ZnO, Zn(O,S), ZnSe, (Zn,Mg)O, and In_2S_3. The latter has received much attention with the $CuInSe_2$ (CIS) and $Cu(In,Ga)Se_2$ (CIGS) absorber as a Cd-free material.[129,130] High efficiencies have been reported for an In_2S_3 buffer layer deposited at substrate temperatures between 160 and 220 °C using indium acetylacetonate and hydrogen sulfide precursors. An efficiency of 10.8% (open-circuit voltage, V_s 592 mV; fill factor, 62%; current density, 29.5 $mAcm^{-2}$) has been achieved for a module area of $30 \times 30\ cm^2$. For laboratory cells, an efficiency of 14.9% was demonstrated in 2003[130] and a subsequent improvement to 16.4% was also reported.[131] Recently, Mughal *et al.* published a comprehensive review on In_2S_3 deposition techniques for CIS, CIGS, and CdTe thin film solar cells and ALD buffer layers performed very well compared to other techniques.[132] Spatial ALD has also been successfully used for fast deposition of different buffer, blocking, and interface layers, according to a recent review by Munoz-Rojas and MacManus-Driscoll.[133] $Zn_{1-x}Sn_xO_y$ is a new ALD-made buffer material reported recently by Lindahl *et al.* (Fig. 10).[134] Efficiencies of up to 18.0% were measured for CIGS cells. Even better results have been reported with Zn_xTi_yO buffer layer (efficiency > 20%.[135]

Sinha *et al.* concluded in a recent review paper that it is not an exaggeration to claim that ALD-grown buffer layers would completely replace the state-of-the-art CdS buffer layers in the near future. Scaling up this technology will make ALD feasible for the industrial production of thin film solar cell modules.[12]

B. Crystalline silicon

In order to utilize the full potential of solar cells fabricated on n-type silicon, it is necessary to achieve excellent passivation on B-doped emitters. ALD has been studied

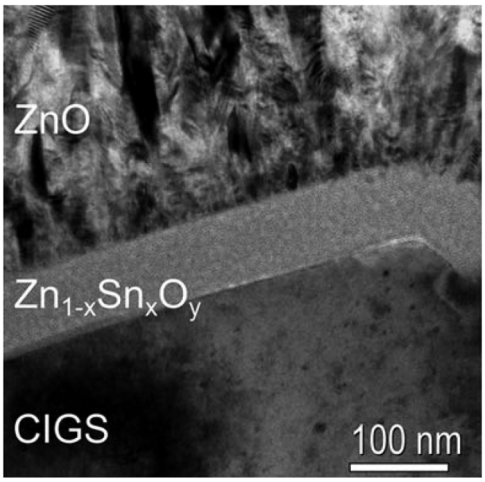

FIG. 10. Bright-field TEM image of $Zn_{1-x}Sn_2O_y$ buffer layer grown on CIGS substrate for 2000 cycles. Reprinted with permission from Lindahl *et al.*, Prog. Photovolt. Res. Appl. **21**, 1588 (2013). Copyright 2013, John Wiley and Sons.

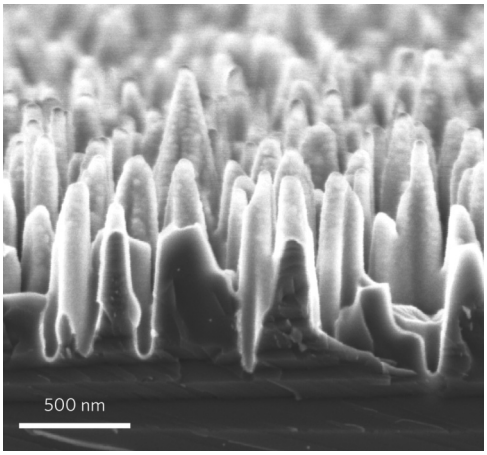

FIG. 11. Scanning electron microscopy (SEM) cross-sectional image of a black silicon surface. Reprinted with permission from Savin *et al.*, Nat. Nanotechnol. **10**, 624 (2015). Copyright 2015, Springer Nature.

because it provides high-quality dielectric films at low processing temperatures. Agostinelli *et al.*[136] showed that low surface recombination velocities can be obtained by thin thermal ALD Al_2O_3 layers on p-type silicon wafers. Thus, low surface recombination is achieved by means of field-induced surface passivation due to a high density of negative charges near the Al_2O_3/c-Si interface. Benick *et al.*[137] used negative-charge dielectric Al_2O_3 fabricated using plasma-enhanced ALD as a front surface passivation layer on high-efficiency n-type silicon solar cells, demonstrating a conversion efficiency of 23.2%. These results indicate that highly doped p-type Si surfaces can be passivated as effectively as highly doped n-type surfaces.[138,139] Later, Dingemans and Kessels[140] showed both experimentally and by simulations that the surface passivation can also be related to a suitably low interface defect density in combination with the field-effect passivation induced by a negative fixed charge density present in the alumina film at the interface. The behavior of plasma-enhanced ALD Al_2O_3 was compared to SiO_2, a-Si:H, and as-deposited a-SiN_x:H, and it was demonstrated that Al_2O_3 provides an excellent level of surface passivation on highly B-doped c-Si with doping concentrations around 10^{19} cm^{-3}.[139] Annealing improves passivation, and for thermal ALD Al_2O_3, the key effect of annealing is the increase of Q_f (negative fixed interface charge), whereas for plasma ALD Al_2O_3, the chemical passivation improves dramatically.[140] The thermal stability in conjunction with the long term and UV stability are prerequisites for the application of Al_2O_3 passivation of solar cells manufactured in high volume. It has also been demonstrated that the application of an ultrathin aluminum oxide capping film can notably improve the silicon surface passivation obtained for low-temperature synthesized SiO_2.[141] This result can again be attributed primarily to a low defect density at the Si/SiO_2 interface. These results indicate the potential for a low-temperature (≤400 °C) passivation process.

Nanostructured silicon (known as black silicon) is an interesting material for photovoltaics where front surface reflection is eliminated (Fig. 11). Nanostructuring enhances the light absorption due to light scattering and trapping effects, improves charge separation due to increased surface area, and improves charge collection due to shorter transport distance. However, charge carrier recombination is also a problem in black silicon. A recent paper reports that high efficiency (22.1%) can be obtained when the surface is coated and thereby passivated with a conformal ALD Al_2O_3 layer.[142]

For ALD to become commercially viable in the PV industry, high throughput processing methods are needed. Two approaches have been taken by the ALD tool industry: optimization of multiwafer batch processing with temporal pulsing and development of spatial ALD. Multiwafer batch processing is a traditional technology and through proper optimization and design of reactors, several ALD tool vendors claim to meet the PV industry's high-quality and throughput demands with over 6000 wafers/h throughput. Spatial ALD reactors are quite new and the PV industry has been a major motivator for their development. High deposition rates have been reported for selected oxides (up to 1.2 nm/s for Al_2O_3).[143] In addition, spatial ALD Al_2O_3 layers can achieve the same level of passivation quality and uniformity on p-type silicon as equivalent temporal ALD Al_2O_3 layers.[144] In contrast, on n-type silicon, the spatial ALD Al_2O_3 layers do not reach the same passivation quality as conventional ALD Al_2O_3 films.

C. Dye-sensitized solar cells

The dye-sensitized solar cells consist of a photosensitizer attached to a mesoporous wide-bandgap semiconductor (TiO_2, ZnO), electrolyte, and back and front electrodes (Fig. 12). The semiconductor that works as a photoanode is usually composed of 10–30 nm TiO_2 nanocrystals deposited on TCO as a thick (5–15 μm) mesoporous layer (by the doctor blade method, for example).[145]

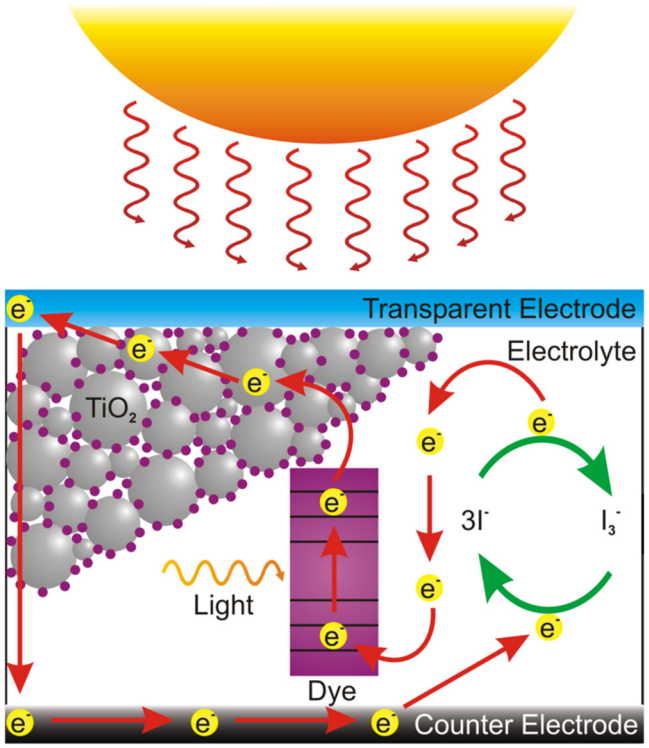

FIG. 12. Schematic representation of a dye-sensitized solar cell showing the flow of electrons from dye via mesoporous TiO_2 to electrodes, electrolyte, and back to dye (Wikimedia Commons, https://commons.wikimedia.org/wiki/File:Dye_Sensitized_Solar_Cell_Scheme.png#file).

One problem that limits the performance of DSSC is the immediate electron recombination, viz., the photoactivated electron of the dye molecule does not transfer to the semiconductor but recombines with the whole. The electron transfer dynamics have been widely studied and are well-understood.[146] In 2006, it was shown with ZnO/Al_2O_3 and ZnO/TiO_2 core-shell nanowires that an ALD Al_2O_3 layer less than 1 nm thick on TiO_2 effectively blocks the electron back-transfer but decreases the efficiency.[147] This phenomenon was later studied with traditional DSSC structures. The results are somewhat difficult to interpret because the actual film thicknesses are not known and instead are reported as numbers of ALD cycles applied. If thickness numbers are given, they have been estimated based on the normal 1 Å/cycle rate reported for the TMA water process. However, there might be some surface inhibition or surface-enhanced growth depending on the TiO_2 surface preparation. It is obvious that after one ALD cycle, a submonolayer is formed and the layer contains holes enabling liquid electrolyte to contact TiO_2.[148] However, it has been shown that even one ALD cycle of Al_2O_3 results in a barrier that slows down electron injection from the singlet excited state of RuN3 dye and decreases the overall injection efficiency. With more than three ALD cycles of Al_2O_3, the triplet state injection is also suppressed, indicating a shift in the TiO_2 density of states.[149] TEM analysis reveals that the Al_2O_3 growth is surface-enhanced and after three cycles, the film thickness is already significant (Fig. 13). The increased distance between the dye and TiO_2 is clearly one reason for the suppression of the electron transfer.

The impact of thin Al_2O_3 films proves to be even more complicated when considering the results obtained using different TiO_2 nanoparticle film thicknesses. For cells containing thick TiO_2 films, the importance of injection and charge collection efficiencies is different than for thin films. Palomares *et al.*[150] reported that on 4-μm thick TiO_2 films, the sol-gel AlO_x coating did not affect short-circuit current density, whereas on 8-μm thick TiO_2 films, the J_{SC} value increased by 30%. Lin *et al.*[151] used one-cycle ALD Al_2O_3 coating on 12-μm thick TiO_2 film and obtained 8% and 13% improvements in J_{SC} value and efficiency, respectively. Thus, the results indicate that Al_2O_3 barrier layers improve cell performance only in the case of thick TiO_2 electrodes.

Chadiran *et al.*[152] have studied ALD Ga_2O_3, ZrO_2, Nb_2O_5, and Ta_2O_5 films as the electron back-transfer blocking layers. They found that thin Ga_2O_3 and ZrO_2 layers (two ALD cycles) clearly improved the short-circuit current density (Fig. 14). Thicker films yielded worse values than the uncoated mesoporous TiO_2 particles. One or two ALD cycles of Nb_2O_5 and Ta_2O_5 did not have a significant effect, and application of more ALD cycles was detrimental. A subnanometer-scale thin ALD Ga_2O_3 layer turned out to be the best blocking material and a record high open-circuit potential was achieved.[153] The conclusion of the research was that the insulating properties of the blocking material were not significant factors. In contrast, properties such as conduction band position, oxidation state of the metal in the oxide, and surface isoelectric properties must be taken into account.

The TiO_2 photoanode can also be a thin film on a dielectric substrate. Hamann *et al.*[154] used silica aerogel as a template to obtain a high surface area ALD TiO_2 photoanode film. They found that the thickest film (12 nm) was the most efficient. Chadiran *et al.* have studied the critical thickness of ALD TiO_2 films on mesoporous SiO_2 particles.[155] The efficiency of a cell increased strongly with increasing TiO_2 thickness from 1 to 8 nm after which it became saturated.

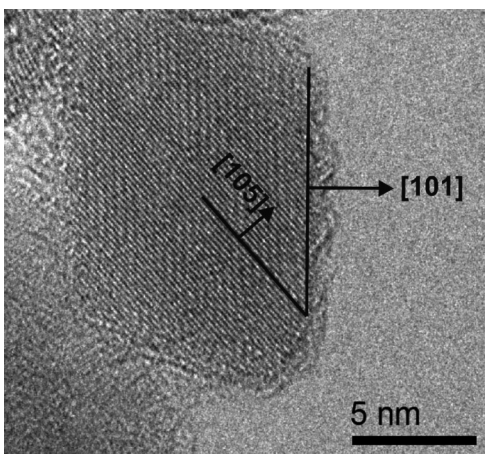

FIG. 13. High-resolution TEM image of a TiO_2 nanoparticle coated with three ALD cycles of Al_2O_3. Reprinted with permission from Antila *et al.*, J. Phys. Chem. C **133**, 16720 (2011). Copyright 2011, American Chemical Society.

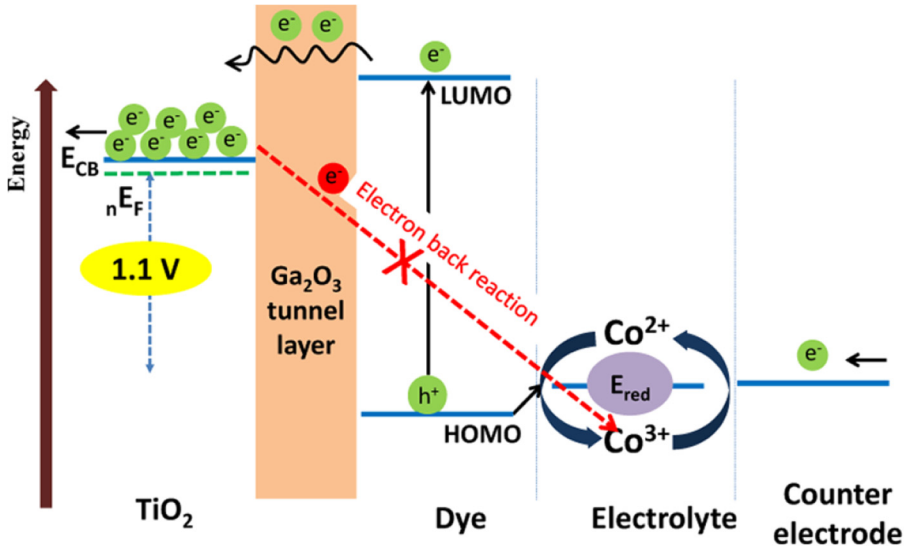

FIG. 14. Schematic representation of the function of the thin ALD Ga_2O_3 blocking layer in DSSC. Reprinted with permission from Chandiran *et al.*, Nano Lett. **12**, 3941 (2012). Copyright 2012, American Chemical Society.

The optimum thickness was ~6–8 nm, which ensured fast electron transport.

One-dimensional TiO_2 and ZnO in the form of nanorods, nanowires, nanobelts, and nanotubes have attracted much attention as photoanodes in dye-sensitized solar cells. The idea is that the 1D oxide structures can provide direct and rapid electron transport to the electron-collecting electrode. Secondly, the traditional nanoparticle-based DSSCs have numerous grain boundaries and surface defects, which increase the charge recombination from photoanode to electrolyte while the 1D nanocrystals are expected to be less defective. The solar cell experiments have shown, however, that the efficiencies of the cells exploiting 1D TiO_2 electron transporters are clearly lower than those obtained with mesoporous TiO_2 nanoparticles.[156,157] A simple explanation of this is the 1D materials provide smaller surface area when compared to particles. In other words, faster reaction kinetics (fast electron transport, long electron lifetime, and less recombination) achieved using the 1D materials do not compensate for the decreased absorption caused by the specific surface area decrease.

ZnO is another wide-bandgap (ca 3.3 eV) metal oxide that much research has been focused on as an alternative to TiO_2 for DSSC applications. The conduction band edge of ZnO is very close to that of TiO_2 and, moreover, it has an electron mobility 2 orders of magnitude higher in the bulk (200–300 $cm^2\,V^{-1}\,s^{-1}$) than in TiO_2.[158] ALD-made ZnO nanotubes templated with anodized alumina previously were studied in DSSC in 2007.[159] The surface area increment was three times higher or more as compared to planar surfaces. External quantum efficiency was 1.5%, which is typical for pure ZnO as the active material. The combination of ZnO with other nanomaterials, such as TiO_2, SiO_2, and ZrO_2 in core–shell structures or buffer layers results in improved electron transport and increased stability of the device leading to an efficiency around 7%.[160] Chadiran *et al.*[161] also studied thin ALD ZnO layers deposited on mesoporous SiO_2 particles and made a comparison to TiO_2 films. The optimum ZnO film thickness was around 5 nm, and the power conversion efficiency was at the same level as that of TiO_2 film. The comparison between ZnO and TiO_2 revealed differences in photo-electrical behavior. The higher electron transport rate contributed to performance of ZnO films, but in the case of TiO_2, the low recombination rate, higher dye loading, and fast electron injection that mainly influenced performance.

Yet another application of ALD in DSSC is the use of a TiO_2 blocking layer on the transparent conductor. Fluorine-doped tin oxide (FTO) transparent conducting electrodes were coated with thin (5–10 nm) ALD TiO_2 for use in organic dye (Y123) and cobalt bis(bipyridine pyrazole) complex based DSSC.[162] The ALD blocking layer promoted a decrease in the dark current, owing to retarded recombination between the FTO and the cobalt electrolyte. It was shown that ZnO and TiO_2 can be used in DSSCs as active layers, photoanodes, buffer layers, transparent conducting oxides, hole-blocking layers, and intermediate layers. Doping is essential to tailor the material properties for each application. Doping of these oxides has been widely studied, as presented in a recent review, and there is great potential for applying ALD to this field.[163]

A breakthrough in solid state DSSCs was made when $CH_3NH_3PbI_3$ perovskite was applied on a mesoporous TiO_2 layer (Fig. 15). The high efficiency increased rapidly, now exceeding 22% in small cells and approaching 20% in centimeter-scale cells.[165,166] Low-cost, high-efficiency perovskite solar cells are now regarded as one of the most promising next-generation photovoltaic technologies. However, there are still many challenges to address before the perovskite solar cells can be used on a larger scale, the main ones being instability, toxicity and large-scale production issues as discussed by Grätzel.[164,165] $CH_3NH_3PbI_3$ is degraded in humid conditions. ALD may be useful for protecting the perovskite or the

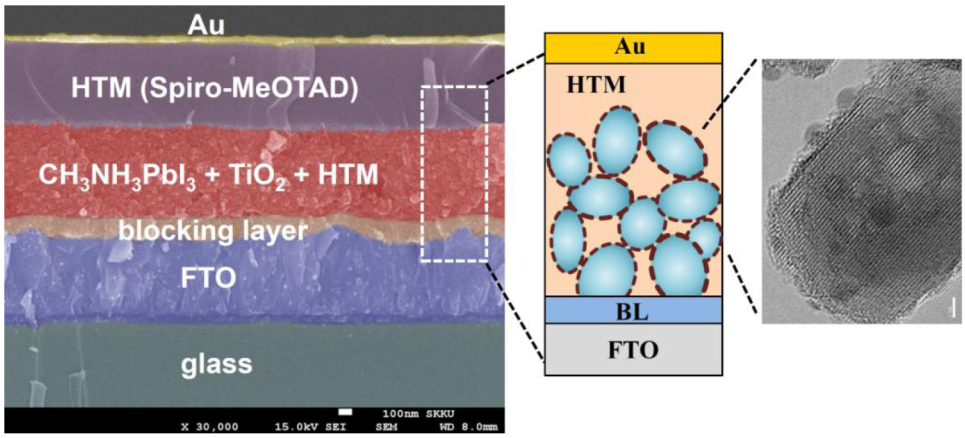

FIG. 15. Cross-sectional SEM image of perovskite-sensitized solid state solar cell showing perovskite nanodots deposited on the mesoscopic TiO_2 scaffold acting as an electron extraction and transport layer. Reprinted with permission from Grätzel and Park, Nano **9**, 1440002 (2014). Copyright 2014, World Scientific Publishing.

whole cell.[11] ALD has been utilized in perovskite DSSC as a blocking layer on TiO_2 nanoparticles.[167] A thin (2 nm) TiO_2 layer can block the electron back-reaction effectively, both from FTO and TiO_2 surfaces. Thin compact oxide layers (TiO_2, ZnO, SnO_2, NiO) can also serve other functions such as an electron or hole transport layer and hole blocking layer.[168–170] Significant improvements have also been reported in cell performance when a thin ALD Al_2O_3 film was introduced between the perovskite layer and metal electrode. The enhancement in charge collection was attributed to the electron blocking effect of the Al_2O_3 layer.[171] Application of ALD layers is usually done prior to perovskite deposition, but recently, deposition directly on perovskite absorbers has been reported, with the goal of replacing organic electron and hole transport layers with ALD metal oxides.[170]

An ALD process for $CH_3NH_3PbI_3$ perovskite may be attractive because it could enable deposition of conformal layers on nanostructured surfaces. No such process exists, but an indirect route has been demonstrated by converting ALD PbS into PbI_2 using iodine gas in a closed system. The PbI_2 is then converted to $CH_3NH_3PbI_3$ by dipping in methylammonium iodide.[172] Popov *et al.*[173] took this process one step further, depositing lead iodide by ALD and then converting it to the perovskite by a vapor phase process.

Perovskite solar cells are also promising candidates as flexible, lightweight energy supply systems for wearable devices. Kim *et al.* published a bendable and efficient (power conversion efficiency 12.2%) perovskite solar cell based on indium-tin oxide on polyethylene naphthalate that was coated with a 20 nm thick TiOx compact layer by plasma-enhanced ALD.[174] The following $CH_3NH_3PbI_{3-x}Cl_x$ absorber layer and 2,2′,7,7′-*tetrakis*(N,N-di-*p*-methoxyphenyl-amine)-9,9′-spirobifluorene (spiro-MeOTAD) hole conductor layer were prepared by spin-coating.

V. 2D MATERIALS

Two-dimensional (2D) materials have received great attention after the discovery of graphene, a single atomic layer of carbon, in 2004. The layered crystal structure enables 2D materials to be isolated as stable, ultrathin layers and gives them unique, thickness-dependent properties. TMDC (Fig. 16) form a highly promising group of 2D materials, which includes semiconductors with different bandgaps as well as semimetals and metals.[17,176–179] The semiconducting TMDCs, such as MoS_2 and WSe_2, have attracted immense attention during the last years. They show exciting, thickness-dependent changes in the nature and magnitude of the bandgap as well as strong photoluminescence, excitonic effects and spin-orbit splitting in monolayer form.[17,176] TMDCs have already shown great promise for serving various functions in optoelectronics, including absorption of light in photodetectors[180,181] and photovoltaics,[182] emission of light in lasers[183] and light-emitting diodes[180,184] as well as hole/electron transport layers.[182] Nevertheless, scalable deposition techniques producing

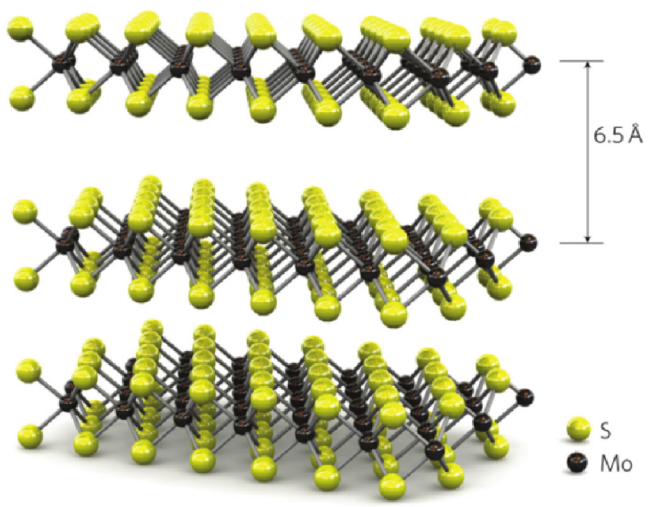

FIG. 16. Crystal structure of TMDCs as exemplified by MoS_2 (2H phase). The covalently bonded chalcogen-metal-chalcogen structure is commonly denoted monolayer. The monolayers are held together only by weak van der Waals forces. Reprinted with permission from Radisavljevic *et al.*, Nat. Nanotechnol. **6**, 147 (2011). Copyright 2011, Springer Nature.

uniform, continuous films of controlled thickness are required for the use of TMDCs in industrial applications. Therefore, ALD is being increasingly studied for the deposition of TMDCs. Herein, we give an overview of TMDCs deposited by ALD focusing on the deposition chemistry as well as three crucial factors regarding their properties and applications: the crystallinity, thickness, and morphology of the deposited films. The ALD-grown TMDCs are briefly introduced in the text and reported ALD TMDC processes are tabulated at the end of the section for the reference. Finally, we discuss the few demonstrated applications and the considerable application potential of ALD-grown TMDCs in optoelectronics.

Most ALD studies of TMDCs have concentrated on MoS_2, the prototypical and most commonly studied TMDC. MoS_2 has properties suitable for many semiconductor applications, such as an optical bandgap ranging from 1.3 (indirect, in bulk) to 1.9 eV (direct, as monolayer), and reasonable charge carrier mobility up to about 200 $cm^2 V^{-1} s^{-1}$.[176,185] In most ALD studies, either $MoCl_5$ or $Mo(CO)_6$ has been used as the molybdenum precursor. Several groups have examined the $MoCl_5 + H_2S$ process at deposition temperatures of 150–500 and even up to 900 °C. Quite different results, including growth rates varying from 0.5 to 6 Å/cycle,[186–190] have been obtained depending on the temperature and other experimental conditions. At high temperatures, Kim *et al.*[191] observed the growth to terminate to three (500 °C), two (600–700 °C), or even one monolayer (900 °C) after a sufficient number of ALD cycles was applied. Furthermore, some publications have noted significant nonuniformity of the films deposited using $MoCl_5$ and H_2S,[19,186,192] which may suggest unwanted etching of the deposited MoS_2 films by $MoCl_5$. Surprisingly, to the best of our knowledge, saturation of the surface reactions in the $MoCl_5 + H_2S$ process has not been tested.

The films deposited by the $MoCl_5 + H_2S$ process are crystalline as deposited,[186–195] although further improvement of crystallinity by postdeposition annealing in S or H_2S atmosphere has been reported.[187,193] The grain size usually varies from 10 to 200 nm depending on growth conditions, film thickness, and morphology, the largest grains usually seen in thicker and rougher films.[189,190,192,194,195] The morphology of MoS_2 films grown by the $MoCl_5 + H_2S$ process depends on factors such as substrate, temperature, and thickness. Islands [Fig. 17(a)][187,190] or continuous films[191] of single monolayer thickness, smooth MoS_2 films with thicknesses of a few monolayers to 10 nm (Refs. 187, 188, 190, and 193) [Fig. 17(b)], and rough films thicker than 10 nm have been demonstrated.[186,192]

The use of the other common molybdenum precursor $Mo(CO)_6$ is limited by its poor thermal stability (reported onset of decomposition from 110 to 250 °C).[19,196–199] Various sulfur precursors, including H_2S,[198,200,201] H_2S plasma,[199,202,203] $S(SiMe_3)_2$,[204] MeSSMe (dimethyldisulfide),[197,205–207] EtSSEt (diethyldisulfide),[208] and HSEtSH (1,2-ethanedithiol)[196] have been used with $Mo(CO)_6$. Despite the low deposition temperatures, the aforementioned sulfur precursors excluding $S(SiMe_3)_2$ have been found reactive enough, showing saturating growth rates above 0.5 Å/cycle.[197–200,202,207] In contrast, Jeon *et al.*[208] reported that SEt_2 did not enable film growth even at 250 °C, which may be due to its structure lacking either protons to donate (as in H_2S and HSEtSH) or ability to form radicals by facile bond cleavage like the disulfides MeSSMe and EtSSEt. H_2S plasma, which produces H_2S^+, H radicals, different S_xH_y species, and various allotropes of elemental sulfur,[209,210] is thought to be the most reactive of the sulfur precursors. HSEtSH differs from the other reported sulfur precursors in that the alkyl chain between the thiol groups is incorporated into the resulting hybrid molybdenum thiolate films.[196,211]

Due to the limited thermal stability of $Mo(CO)_6$, the films deposited at 100–200 °C are usually amorphous, except when using H_2S plasma.[199,202,203] This may be attributed to the greater reactivity of plasma-activated species or ion bombardment effects. As an exception, the MoS_2 films deposited at 100 °C using $Mo(CO)_6$ and MeSSMe were partially nanocrystalline on carbon fiber paper,[207] whereas the films

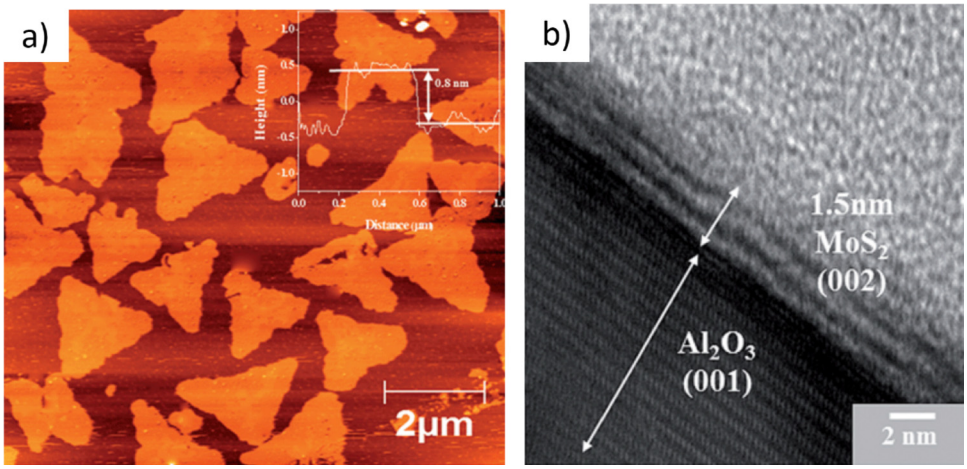

FIG. 17. (a) AFM image of monolayer islands after an MoS_2 film grown on sapphire using $MoCl_5$ and H_2S at 300 °C was annealed at 800 °C. (b) Cross-sectional TEM image of the same film prior to annealing (continuous three monolayer film). Reprinted with permission from Tan *et al.*, Nanoscale **6**, 10584 (2014). Copyright 2014, Royal Society of Chemistry.

deposited on gold and silicon were reported to be amorphous.[197,205] Using $Mo(CO)_6$ and EtSSEt, Jeon *et al.*[208] were able to deposit crystalline, five-monolayer thick MoS_2 films at 250 °C with grain sizes as large as 100 nm when using a diethylsulfide (SEt_2) pretreatment to decrease the nucleation density. However, the process did not saturate due to the decomposition of $Mo(CO)_6$.

High-temperature annealing treatments at 500–900 °C using Ar,[197,198,206] S,[204] or H_2S[198,202] atmospheres have been used to crystallize MoS_2 films. In this way, uniform MoS_2 films of a few monolayers in thickness to crystallize MoS_2 films grown using $Mo(CO)_6$ have been demonstrated on up to 4 in. wafers.[198] Small grain sizes of 10 nm or below and high temperatures may limit the use of these processes, however.[197,198] The hybrid molybdenum thiolate films deposited using $Mo(CO)_6$ and HSEtSH could be converted into crystalline MoS_2 at only 350 °C in an H_2S/N_2 atmosphere.

To resolve issues such as poor reproducibility and possible etching when using $MoCl_5$, as well as the difficulty in obtaining crystalline films with $Mo(CO)_6$, other molybdenum precursors have been investigated. Another molybdenum halide, MoF_6, has been used with H_2S.[212,213] The rough films deposited at 200 °C (~0.5–0.8 Å/cycle) were amorphous as deposited, but could be crystallized by a mild annealing treatment at 350 °C in H_2.[212] Further in-depth studies of film structure revealed that annealing at a higher temperature of 600 °C in H_2 or H_2S ambient is beneficial for producing a well-ordered MoS_2 structure with a grain size of 4–10 nm.[213] Mattinen *et al.*[19] introduced the $Mo(thd)_3 + H_2S$ process, which enables deposition of rough, crystalline MoS_2 films at reasonably low temperatures of 250–350 °C. However, the saturated growth rate was only 0.025 Å/cycle at 300 °C and the grain size of the films was rather small, approximately 10–30 nm. Sharma *et al.*[214] used $Mo(N^tBu)_2(NMe_2)_2$ with H_2S plasma to grow MoS_2 films at 150–450 °C with high saturated growth rates (~0.7–3 Å/cycle). The crystallinity and morphology could be tuned by adjusting deposition conditions: rough, crystalline MoS_2 films were deposited at 300–450 °C, while predominantly amorphous films resulted at lower temperatures. At 450 °C, the films initially grew with the 2D layers aligned parallel to the substrate, but the films roughened with increasing thickness.

$Mo(NMe_2)_4$ was introduced as a low-temperature precursor that enables growth of amorphous films at temperatures as low as 50 °C with H_2S (Ref. 215) or HSEtSH (Ref. 211). Annealing the hybrid films deposited using HSEtSH for three ALD cycles produced films composed of randomly oriented MoS_2 crystallites below 5 nm in size when the annealing was performed in H_2 at 450 °C, whereas annealing in Ar at 800 °C resulted in a mainly monolayer film composed of 10–20 nm MoS_2 grains with carbon inclusions between the MoS_2 grains.[211] The films grown with H_2S were annealed at 1000 °C in an S atmosphere resulting in smooth films with an apparent grain size as large as 100–200 nm as estimated from an AFM image.[215]

$MoSe_2$ is a semiconducting TMDC with a slightly smaller optical bandgap of 1.1 (bulk) to 1.6 eV (monolayer) and higher electrical conductivity compared to MoS_2. Few ALD studies exist on $MoSe_2$ and other selenides, due to the limited availability of good selenium precursors. H_2Se is much more toxic than H_2S and alkylselenides such as diethylselenide (SEt_2) are considered to be rather unreactive under ALD conditions. Pore *et al.*[216] introduced alkylsilyl compounds of selenium and tellurium as efficient ALD reactants. These reactants are also starting to be used for TMDCs as relatively safe selenium precursors (telluride TMDCs have not yet been deposited by ALD). Deposition of $MoSe_2$ has been attempted using either $Mo(CO)_6$ or $MoCl_5$ with $Se(SiMe_3)_2$. The films deposited with $Mo(CO)_6$ at 167 °C were amorphous and characterized as oxyselenides,[217,218] while those deposited using $MoCl_5$ at 300 °C were crystalline $MoSe_2$ with a rough, flaky morphology.[217] However, saturation was not examined for either process.

ReS_2 is an intriguing TMDC with some major differences compared to the commonly studied group 6 (Mo, W) TMDCs. ReS_2 has anisotropic properties in the 2D-plane due to its low-symmetry structure and it is considered to have very weak interlayer coupling leading to properties that are nearly independent of thickness. For example, the direct bandgap is approximately 1.5 eV regardless of film thickness.[178] Hämäläinen *et al.*[219] reported deposition of ReS_2 films using $ReCl_5$ and H_2S with crystalline ReS_2 deposited between 200 and 500 °C with growth rates of 0.9–0.2 Å/cycle, respectively. The morphology could be tuned by deposition temperature as well as film thickness. Most of the examined films were rough, but the existence of a thin initial layer aligned parallel to the amorphous ALD Al_2O_3 substrate suggests the possibility of depositing smooth, ultrathin films.

SnS_2 is included here with the TMDCs although tin is not a transition metal. This is because SnS_2 shares the 1T-type crystal structure with several TMDCs. SnS_2 has recently emerged as an alternative to MoS_2 and other semiconducting TMDCs, as it exhibits a reasonable bandgap (~2.2 eV in bulk, 2.6 eV as monolayer), good performance in applications such as FETs and photodetectors, as well as nontoxicity, earth abundance, and high mobility of tin atoms.[220] ALD of SnS_2 films was initially studied by Thimsen *et al.*,[221,222] Hägglund *et al.*,[223] and Ham *et al.*[224] using $Sn(NMe_2)_4$ and H_2S. Recently, the process has been studied in detail by Jeon's group.[225–229] Mattinen *et al.*[230] introduced the $Sn(OAc)_4 + H_2S$ process as an alternative for depositing SnS_2 films. Reasonable growth rates of 0.2 Å/cycle[229] and 0.5–0.6 Å/cycle[224,225] with saturative behavior were observed for the $Sn(OAc)_4$+H_2S and $Sn(NMe_2)_4$+H_2S processes, although they are both limited to a very narrow temperature range around 150 °C.

SnS_2 films deposited using either of the processes at 150 °C are amorphous below a thickness of approximately 10 nm.[225,230] To improve the crystallinity, low-temperature annealing procedures have been investigated. In an $S/H_2/Ar$ atmosphere, 300 °C was found to be optimal for a 12-nm SnS_2 film [Figs. 18(a) and 18(b)],[226] whereas in an H_2S/Ar atmosphere, a three-step procedure first at 250 °C, then at 300 °C, and finally at 350 °C proved even better for a 3.6-nm (6-monolayer) film.[227] For a 3.5-nm film deposited by the $Sn(OAc)_4 + H_2S$ process, the best crystallinity was obtained

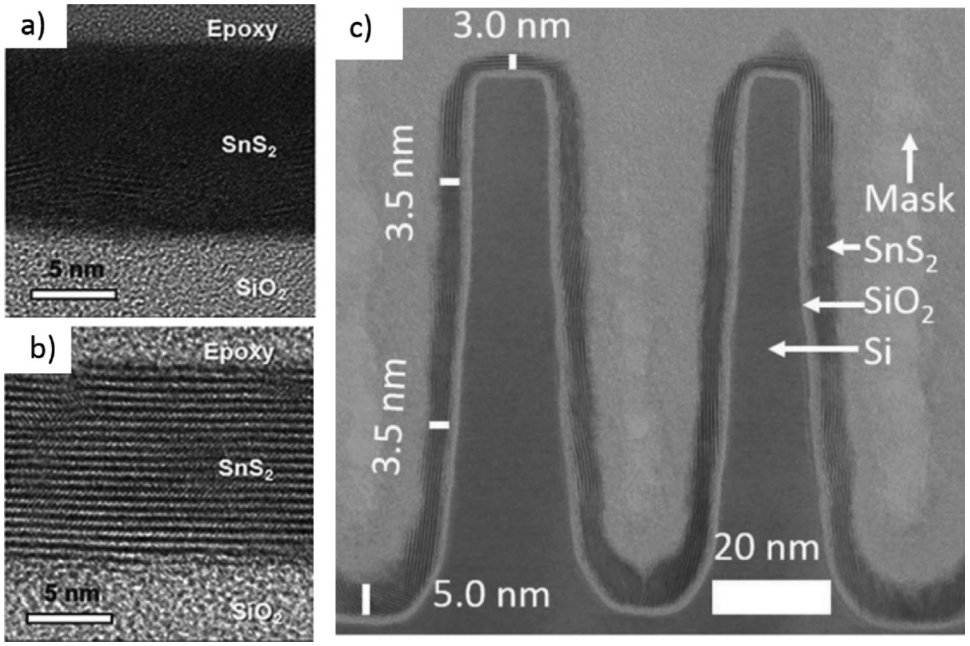

FIG. 18. Cross-sectional TEM images of (a) a mostly amorphous SnS_2 film as-deposited using $Sn(NMe_2)_4 + H_2S$ at 150 °C, (b) a crystalline SnS_2 film after annealing the previous film at 300 °C in an $S/H_2/Ar$ atmosphere, and (c) a crystalline SnS_2 film conformally deposited on a trench structure using $Sn(OAc)_4$ and H_2S at 150 °C followed by H_2S/N_2 annealing at 250 °C. (a) and (b) Reprinted from Lee *et al.*, AIP Adv. **7**, 025311 (2017). Copyright 2017, Authors, distributed under a Creative Commons Attribution (CC BY) License. (c) Reprinted with permission from Mattinen *et al.*, Small **14**, 1800547 (2018). Copyright 2018, John Wiley and Sons.

after annealing at 250 °C in an H_2S/N_2 environment.[230] The film deposited by the $Sn(OAc)_4 + H_2S$ process remained continuous and fairly smooth even when it crystallized on a nanoscale trench structure with sharp features [Fig. 18(c)]. Higher annealing temperatures could not be used for SnS_2 because of reduction or sublimation of the film.[226,227,230] Another possibility is to first deposit an SnS film using $Sn(NMe_2)_4$ and H_2S at 170 °C and then convert the SnS film to SnS_2 at 450 °C in H_2S.[229] As shown by the low annealing temperatures enabled by the high mobility and diffusivity of tin, SnS_2 may be beneficial over other TMDCs in achieving highly crystalline films at temperatures compatible with many applications and substrates, such as back-end-of-line microelectronics processing (approximately <400 °C).[231] The two-step approach where an initially amorphous film is crystallized by mild annealing enables deposition of smooth and continuous films from only two monolayers[230] up to tens of nanometers in thickness.[229] This has been difficult to achieve with other TMDCs.

TiS_2 is highly conductive and either semimetallic or a small bandgap semiconductor,[177] in contrast to the other TMDCs deposited by ALD that have sizeable bandgaps (1–2.5 eV). TiS_2 has been deposited using $TiCl_4$ and H_2S, either at 400–500 °C (Ref. 232) or at 75–250 °C.[233] The films deposited in the lower temperature range were weakly crystalline,[233] whereas those deposited at 400 °C were highly crystalline.[232] Interestingly, at 400 °C, the process resulted in very different growth on different substrates in terms of growth rate, composition, crystallinity, and morphology. For example, no film growth was found on silicon with native oxide, whereas a very rough film consisting of up to 1-μm wide flakes formed on soda lime glass. A relatively dense film consisting of columnar TiS_2 grains, atypical for TMDCs, was obtained on zinc sulfide.

WS_2 is often studied as an alternative to MoS_2 due to their fairly similar properties.[176] Initial ALD studies on WS_2 by Scharf and his team[234–236] focused on deposition of ten to hundreds of nanometer thick, rough films using WF_6 and H_2S. However, it was found that the growth did not proceed unless zinc was present either in a substrate (ZnS) or periodically supplied as $ZnEt_2$ pulses. When an ultrathin ZnS layer was used, the resulting films were nanocrystalline and contained ZnF_2 and ZnS inclusions. Periodically applying $ZnEt_2$ pulses instead resulted in a rough film with 50–100 nm wide grains.

Delabie's group found an alternative way to grow WS_2 from WF_6 by adding an H_2 plasma pulse between the WF_6 and H_2S pulses at 300 °C.[236–239] Further studies on the $WF_6 + H_2$ plasma $+ H_2S$ process have examined the nucleation of WS_2 on different substrates,[238] tuning grain size by different parameters[239] as well as the use of WS_2 in FETs on 300-mm wafers,[240] making it the most thoroughly understood TMDC ALD process to date. Remarkably, the process has been shown to deposit continuous films as thin as two monolayers on 300-mm wafers. The substrate and deposition conditions were shown to have a large influence on the film nucleation and growth (Fig. 19). On amorphous ALD Al_2O_3, the nucleation was very rapid and film closure occurred at a nominal thickness of only 1.2 monolayers of WS_2, but the resulting film had a small grain size of 5–20 nm. The nucleation density was smaller on sapphire (α-Al_2O_3) and even smaller on SiO_2, resulting

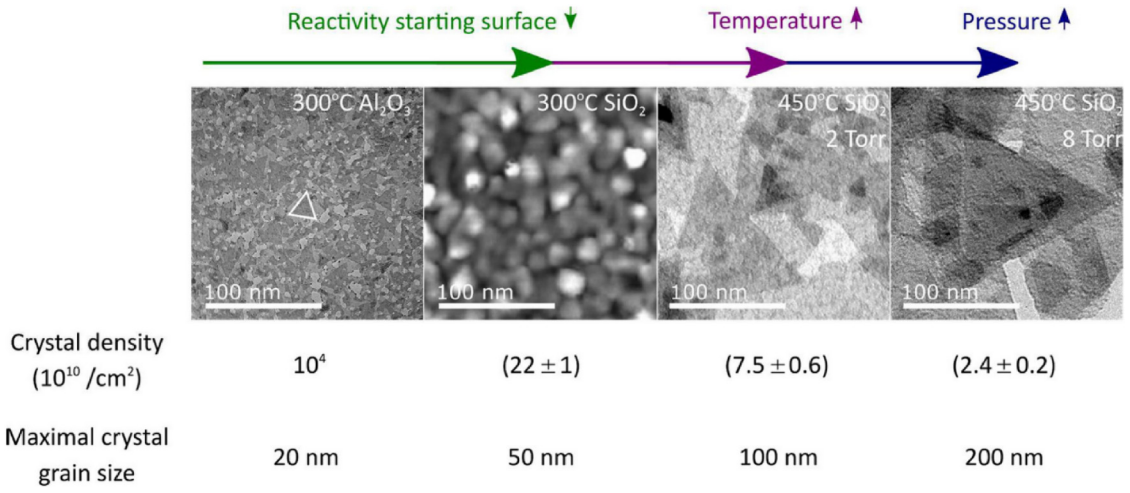

FIG. 19. Plan-view TEM images illustrating tuning of nucleation density and grain size of WS_2 films by changing the starting surface, deposition temperature, and reactor pressure. The films were grown by the $WF_6 + H_2$ plasma $+ H_2S$ process. Reprinted with permission from Groven *et al.*, Chem. Mater. **30**, 7648 (2018). Copyright 2018, American Chemical Society.

in up to 50-nm wide grains on the latter.[238,239] By increasing the deposition temperature as well as reactor pressure, the nucleation could be further hindered and the grain size increased up to 200 nm (average 72 nm) on SiO_2, though at the expense of delayed formation of a continuous film.[239]

In addition to WF_6, other reported processes use tungsten chloride WCl_x with H_2S (claimed to be WCl_5, more likely the more common WCl_6),[241] and $W(CO)_6$ with either H_2S (Refs. 242 and 244) or H_2S plasma.[245] Limited results (no information provided on saturation of the surface reactions) were provided for the $WCl_x + H_2S$ process operated at 390 °C, although the films were reported to be of good quality and continuous at a thickness of only a few monolayers.[241] The WS_2 films grown using $W(CO)_6$ and H_2S at 165–205 °C with a saturated growth rate of 0.2 Å/cycle were amorphous,[242] similar to the analogous MoS_2 process. A much higher growth rate of 3.6 Å/cycle at a much higher temperature of 400 °C was reported by Sun *et al.*,[243,244] but no information on saturation was provided. The films were nanocrystalline and randomly oriented apart from an initial ~5-nm layer approximately aligned with the ZnS/Si substrate. Yeo *et al.*[245] used $W(CO)_6$ with H_2S plasma, demonstrating saturated growth at ~1 Å/cycle for a relatively high deposition temperature of 350 °C. This resulted in nanocrystalline WS_2 films.

WSe_2 has received considerable attention due to its attractive properties including good charge carrier mobility and ambipolar or p-type characteristic, which supplements the typically n-type MoS_2 and WS_2.[246,247] WSe_2 also exhibits unique optical and electrical properties due to its stronger spin-orbit coupling compared to most other TMDCs.[176,246] Two ALD processes have been reported, the first one using WCl_x with H_2Se at 390 °C.[247] No saturation experiments were reported and the growth rate was as high as 5 Å/cycle, which casts doubt on the ALD behavior of the process. Nevertheless, the approximately five-monolayer films deposited by the process were continuous, smooth, and of high crystalline and electrical quality. Park *et al.*[248] used WCl_6 and SEt_2 precursors to produce continuous, high-quality WSe_2 films in a process that terminated to a thickness of five (600 °C), three (700 °C), or even one monolayer (800 °C) depending on the deposition temperature.

While few studies have examined ALD TMDCs for optoelectronic applications, this is likely to change in the future. Guidance on the prospects of ALD TMDCs in optoelectronics may be obtained by considering the crystallinity, morphology, and thickness of ALD-grown TMDCs in

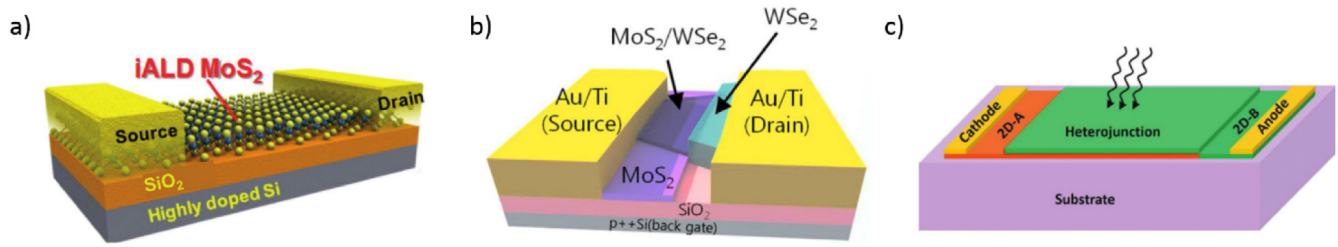

FIG. 20. (a) Schematic of an FET using ALD MoS_2 film as the channel. Reprinted with permission from Jeon *et al.*, Adv. Mater. **29**, 1703031 (2017). Copyright 2017, John Wiley and Sons. (b) Schematic of a p-n diode photodetector using ALD MoS_2 as the n-type material. Reprinted from Kim *et al.*, Sci. Rep. **6**, 18754 (2016). Copyright 2016, Authors, distributed under a Creative Commons Attribution (CC BY) License. (c) Schematic of a 2D-2D heterojunction solar cell. Reprinted with permission from Das *et al.*, Adv. Mater. **31**, 1802722 (2019). Copyright 2018, John Wiley and Sons.

TABLE I. Summary of TMDC films deposited by ALD. One monolayer (ML) of most TMDCs corresponds to approximately 0.6 nm. Morphology is classified as flakes (discontinuous), films (continuous, smooth), or rough films (continuous, rough surface). If grain size cannot be estimated, the film is only denoted crystalline/amorphous. Abbreviations: amorphous (amorp.), annealed (ann.), as-deposited (as-dep.), crystalline (cryst.), field-effect transistor (FET), hydrogen evolution reaction (HER), oxygen evolution reaction (OER), photoelectrochemical (PEC), and supercapacitor (SC).

Precursors	Dep. temperature (post-treatment)	Thickness, morphology (estimated grain size)	Applications	Reference
MoS_2				
$MoCl_5 + H_2S$	300 °C (800 °C in S)	1 ML flakes, 1 ML to 10 nm films (as-dep. ~10 nm, ann. <2 μm)	—	187
	350–450 °C	2 ML to 10 nm films (cryst.)	FET	188
	500–900 °C	1–3 ML films (80–100 nm)	FET, p-n diode	191
	375–475 °C (600–900 °C in S or H_2S)	A few ML films (cryst.)	—	193
	450 °C	1–3 ML flakes (~100 nm) 4–10 ML films	—	190
	420–490 °C	10–50 nm films (20–100 nm)	—	194
	390–480 °C	20–60 nm films (30–120 nm)	Piezoelectric	189
	460 °C	2.5–45 nm films (10–15 nm)	Lubricant	195
	250–325 °C	20–70 nm rough films (10–100 nm)	HER	186
	150–300 °C	5–50 nm rough films (10–300 nm)	Li, Na battery	192
$MoF_6 + H_2S$	200 °C (350 °C in H_2)	~10–100 nm rough films (as-dep. amorp., ann. cryst.)	—	212
	200 °C (400/600 °C in H_2 or H_2S)	~10 nm films (as-dep. amorp., ann. 4–10 nm)	—	213
$Mo(CO)_6 + H_2S$	155–170 °C	10–50 nm films (amorp.?)	Li battery	200
	120–175 °C (500–900 °C in Ar or H_2S)	2 ML to 10 nm films (as-dep. amorp., ann. ~10 nm)	—	198
	200 °C	? nm rough films (~5 nm)	OER	201
$Mo(CO)_6 + H_2S$ plasma	175–225 °C	5–30 nm rough films (15–20 nm)	—	199
	200 °C	10–50 nm films (~5 nm)	SC	203
	200 °C (500–700 °C in H_2S)	5–30 nm rough films (as-dep. 6–10 nm, ann. ~15 nm)	PEC HER	202
$Mo(CO)_6 + S(SiMe_3)_2$	150 °C (800 °C in S)	2–5 ML films (as-dep. amorp.?, ann. ~5–10 nm)	FET	204
$Mo(CO)_6 + MeSSMe$	100 °C (900 °C in Ar)	5–10 nm films (as-dep. amorp., ann. 10 nm)	—	197
	100 °C	2–10 nm films (amorp.)	HER	205
	100 °C	2–15 nm films (<5 nm, partly cryst.)	HER	207
	150 °C (650–700 °C in Ar)	~5–50 nm films (as-dep. amorp., ann. cryst.)	photonic crystal	206
$Mo(CO)_6 + EtSSEt$	250 °C	~5 ML films (100 nm)	FET	208
$Mo(CO)_6 + HSEtSH$	140–190 °C (350 °C in $H_2S + H_2$)	~10 nm films (as-dep. amorp., ann. ~5 nm)	HER	196
$Mo(thd)_3 + H_2S$	250–350 °C	~2–10 nm rough films (10–30 nm)	—	19
$Mo(N^tBu)_2(NMe_2)_2 + H_2S$ plasma	150–450 °C	1 ML flakes to tens of nm rough films (10–50 nm)	HER	214
$Mo(NMe_2)_4 + H_2S$	60–120 °C (1000 °C in S)	3–50 nm films (as-dep. amorp., ann. 100–200 nm?)	FET	215
$Mo(NMe_2)_4 + HSEtSH$	50 °C (300 °C in Ar or H_2, 450 °C in H_2, or 800 °C in Ar)	1–2 ML films (as-dep. amorp., ann. 10–20 nm)	—	211
$MoSe_2$				
$MoCl_5 + Se(SiMe_3)_2$	300 °C	>10 nm rough films (50–100 nm)	—	217
$Mo(CO)_6 + Se(SiMe_3)_2$	167 °C	1–10 nm films (amorp.)	PEC, photocatalysis	217,218
ReS_2				
$ReCl_5 + H_2S$	120–500 °C	~1–100 + nm rough films (10–300 nm)	—	219
SnS_2				
$Sn(NMe_2)_4 + H_2S$	135 °C	~20 nm films (cryst. on Cu_2S)	—	221,222
	60–120 °C	50 nm films (amorp. SnS_2)	—	224
	140–150 °C	50 nm films (~10 nm, SnS_2)		
	160–180 °C	50 nm rough films (~15 nm, SnS)		
	150 °C	2–45 nm films (<10 nm films amorp., thicker cryst.)	—	225
	150 °C (250–350 °C in S + H_2 + Ar)	12 nm (as-dep. 15 nm, ann. 25 nm)	—	226
	150 °C (250–350 °C in H_2S + Ar)	3.6 nm/6 ML (as-dep. partly cryst, ann. ~10 nm)	—	227

TABLE I. (*Continued*.)

Precursors	Dep. temperature (post-treatment)	Thickness, morphology (estimated grain size)	Applications	Reference
	150 °C (300 °C in $S + H_2 + Ar$)	12 nm film (as-dep. partly cryst, ann. cryst.)	FET	228
	170 °C (450 °C in H_2S)	20 or 40 nm films (ann. >40 nm)	FET	229
	90 °C	~5–30 nm (amorp.)	Plasmonics	223
$Sn(OAc)_4 + H_2S$	150 °C (200–350 °C in $H_2S + N_2$)	2–11 ML films (as-dep. amorp., ann. 20–30 nm)	—	230
TiS_2				
$TiCl_4 + H2S$	400–500 °C	50–100 nm rough films (amorp. to 1 μm grains depending on subst.)	—	232
	75–250 °C	3–50 nm films (partly cryst.)	Solar cell	233
WS_2				
$WF_6 + H_2S$	300 °C (500 °C in vacuum)	~250 nm rough film (as-dep. ~10 nm, ann. ~30 nm)	Lubricant	251
	300–350 °C	10–400 nm rough films (5–100 nm)	Lubricant	234,235
$WF_6 + H_2$ plasma $+ H_2S$	250–450 °C	2–5 ML films (~10 nm)	—	236,237
	300 °C	2–5 ML films (5–20 nm)	—	238
	300 °C	4–5 ML film (10–20 nm)	FET	240
	300–450 °C	~1–5 ML flakes, ~2–5 ML films (tunable ~5–200 nm)	FET	239
$WCl_x + H_2S$	390 °C	A few–10 ML (cryst.)	FET	241
$W(CO)_6 + H_2S$	165–205 °C	20–40 nm (amorp.)	Li battery	242
	400 °C	175 nm rough films (~5 nm)	Lubricant	243,244
$W(CO)_6 + H_2S$ plasma	350 °C	3–20 nm films (3–7 nm)	HER, Na battery	245
WSe_2				
$WCl_6 + SeEt_2$	600–800 °C	1–5 ML films (200 nm)	FET	248
	700 °C	3 ML film (cryst.)	Gas sensor	250
$WCl_x + H_2Se$	390 °C	~5 ML film (cryst.)	FET	249

comparison to TMDC films/crystals already used in lab-scale optoelectronic devices. ALD TMDCs have been studied for electronics, in particular field-effect transistors [FET, Fig. 20(a)].[188,191,204,208,215,228,229,239,240,248,249] More rarely, they have also been studied as gas sensors[250] and photodetectors.[248] In all cases, the examined films have been crystalline and smooth and usually from 1 to 5 monolayers in thickness (Table I), properties that are expected to be beneficial for device performance along with large lateral grain size. Good FET performance has been demonstrated for ALD MoS_2,[188,204,208] WS_2,[239,241] and WSe_2,[248,249] whereas the performance of ALD SnS_2 has been modest.[228,229] As an example, charge carrier mobilities on the order of 1–10 $cm^2 V^{-1} s^{-1}$, which are comparable to MoS_2 grown by CVD at 600 °C and above, have been reported for a 2-ML MoS_2 film deposited using $MoCl_5 + H_2S$ at 390 °C,[188] a 5-ML film deposited using $Mo(CO)_6 + EtSSEt$ at 250 °C,[208] and a 4-ML film deposited by the $Mo(CO)_6 + S(SiMe_3)_2$ process at 150 °C followed by annealing in sulfur at 800 °C.[204]

Crystalline, smooth few-layer TMDC films grown by ALD should also be promising for optoelectronic devices such as photodetectors. However, controlling the morphology of ALD-grown TMDCs is challenging and requires further studies to understand why the deposited films are sometimes smooth and in other cases very rough. The only proof-of-concept ALD TMDC photodetector presented to date uses n-type MoS_2 that was grown by ALD on top of an exfoliated p-type WSe_2 flake, performing as a photoresponsive p-n diode [Fig. 20(b)].[248] It should be rather straightforward to also make photoresistive photodetector devices based on ALD TMDCs, as these devices are simpler than the FETs and p-n diodes that have already been demonstrated. Based on the FET studies, ALD MoS_2 and WS_2 can be either n- (Refs. 188, 191, 208, 215, and 241) or p-type,[204,239] while SnS_2 is n-type[228,229] and WSe_2 either p-type[248] or ambipolar.[249] Thus, creating p-n diodes using only ALD-grown TMDCs should also be feasible. Some optoelectronics applications, such as light-emitting devices,[184] often require TMDCs to have a thickness of exactly one monolayer to achieve the direct bandgap (perhaps with the exception of ReS_2) and such devices are usually demonstrated on exfoliated flakes. Thus, they pose two challenges for ALD: deposition of films of uniform monolayer thickness as well as an increase in grain size compared to the existing processes.

Using ALD, TMDCs as ultrathin absorbers in photovoltaics have been demonstrated by Mahuli and Sarkar,[233] who deposited a weakly crystalline, approximately 10-nm thick TiS_2 film on a porous TiO_2 substrate, resulting in a modest power conversion efficiency of 0.57%. Although using mono- to few-layer TMDCs as absorbers may at first seem ineffective, the extraordinary optical properties of TMDCs allows a single 0.6-nm thick TMDC monolayer to absorb approximately 10% of the solar spectrum—as much as a 50-nm layer of Si.[252] ALD would be ideally suited to grow p-n junctions of two 2D materials for a 2D solar cell [Fig. 20(c)], thanks to its excellent scalability and film

uniformity. In the case of 2D materials, the slowness of ALD, which has hindered the use of ALD-grown conventional solar cell absorbers, should not be an issue. Alternatively, ALD TMDC may be grown on top of silicon, for example, for a 3D-2D p-n junction—a design that has already shown efficiencies exceeding 5%.[182,253] Furthermore, the absorber films do not have to be exactly one monolayer thick, which enables using many of the reported ALD TMDC processes, and the relatively low deposition temperatures used in ALD ensures that issues of interdiffusion of the two layers are unlikely. Again, the ALD processes producing smooth, crystalline TMDC layers would likely be the first candidates to be tested in photovoltaics.

VI. SUMMARY AND CONCLUSIONS

Atomic layer deposition has been used since the mid-1980s in the production of the kernel of thin film electroluminescent displays, viz., dielectric and luminescent layers. Although ALD is a slow method, the benefits of ALD in this application include high quality of the films and the potential to deposit the whole dielectric-luminescent-dielectric layer package in one process while simultaneously processing large batches of substrates. Besides the traditional monochrome yellow-black displays, transparent thin film EL displays are produced on an industrial scale.

ALD technology has been heavily adopted in the field of silicon-based microelectronics where it is used to deposit dielectric, metallic, and barrier films. ALD was studied extensively in the 1980s and early 1990s for the deposition of epitaxial III-V semiconductor films. However, there were no breakthroughs in this application area. Because of the dense and high-quality thin films produced, ALD is used widely for passivation and encapsulation purposes. This is also true for all kinds of solar cells—silicon, thin film, dye-sensitized and quantum dot solar cells, and LEDs.

Two-dimensional transition metal dichalcogenides are interesting emerging optoelectronic materials that show desirable properties as single- or few-monolayer thin films. ALD is studied as a potential method for processing them as high-quality, large-area films. More research is needed on the use of ALD for optoelectronic applications, including photodetectors as well as different layers in photovoltaics (absorber and hole extraction layers, for example). While the quality and performance of ALD TMDC films are usually compared to high-quality flakes manufactured by exfoliation or CVD, efforts should also be directed at finding new applications and substrates where the uniformity and conformality of ALD films are crucial.

ACKNOWLEDGMENT

This work has been supported by the Finnish Centre of Excellence in ALD (Academy of Finland Grant No. 284623).

[1]T. Suntola and J. Anson, U.S. patent 4,058,430 (15 November 1977).
[2]R. L. Puurunen, Chem. Vap. Deposition **20**, 332 (2014).
[3]R. O. Törnqvist, J. Antson, J. Skarp, and V.-P. Tanninen, IEEE Trans. Electron Devices **ED-30**, 468 (1983).
[4]M. Leskelä and M. Ritala, Angew. Chem. Int. Ed. **42**, 5548 (2003).
[5]M. Ritala and J. Niinistö, ECS Trans. **25**, 641 (2009).
[6]J.-I. Nishizawa, H. Abe, and T. Kurabayashi, J. Electrochem. Soc. **132**, 1197 (1985).
[7]S. M. Bedair, M. A. Tischler, T. Katsuyama, and N. A. El-Masry, Appl. Phys. Lett. **47**, 51 (1985).
[8]N. Biyikli and A. Haider, Semicond. Sci.Technol. **32**, 093002 (2017).
[9]B. Hoex, J. Schmidt, P. Pohl, M. C. M. van de Sanden, and W. M. M. Kessels, J. Appl. Phys. **104**, 044903 (2008).
[10]N. Tétreault, L.-P. Heiniger, M. Stefik, P. P. Labouchère, É Arsenault, N. K. Nazeeruddin, G. A. Ozin, and M. Grätzel, ECS Trans. **41**, 303 (2011).
[11]K. Deng and L. Li, Adv. Mater. Interfaces **3**, 1600505 (2016).
[12]S. Sinha, D. K. Nandi, S.-H. Kim, and J. Heo, Solar Energy Mater. Solar Cells **176**, 49 (2018).
[13]J. Meyer *et al.*, Appl. Phys. Lett. **94**, 233305 (2009).
[14]H. Choi, H. Jeon, Y. Choi, J. Kim, S. Kim, S. C. Chung, and K. Oh, J. Vac. Sci. Technol. A **34**, 01A121 (2016).
[15]N. Avci, J. Musschoot, P. F. Smet, K. Korthout, A. Avci, C. Detavernier, and D. Poleman, J. Electrochem. Soc. **156**, J333 (2009).
[16]Z. Zhou, N. Zhou, X. Lu, M. ten Kate, D. Valdesueiro, J. R. van Ommen, and H. T. Hintzen, RSC Adv. **6**, 76454 (2016).
[17]M. Chhowalla, H. S. Shin, G. Eda, L.-J. Li, K. P. Loh, and H. Zhang, Nat. Chem. **5**, 263 (2013).
[18]Z. Wang, Q. Jingjing, X. Wang, Z. Zhang, Y. Chen, X. Huang, and W. Huang, Chem. Soc. Rev. **47**, 6128 (2018).
[19]M. Mattinen *et al.*, Adv. Mater. Interfaces **4**, 1700123 (2017).
[20]R. Törnqvist, Displays **13**, 81 (1992).
[21]See: www.beneq.com
[22]C. N. King, J. Vac. Sci. Technol. A **14**, 1729 (1996).
[23]M. Leskelä, W.-M. Li, and M. Ritala, "Semiconductors and semimetals," in *Electroluminescence II*, edited by G. O. Müller (Academic, New York, 1999), Vol. **65**, p.107.
[24]T. Suntola and J. Hyvärinen, Annu. Rev. Mater. Sci. **15**, 177 (1985).
[25]R. Törnqvist and T. O. Tuomi, J. Lumin. **24/25**, 901 (1981).
[26]R. Törnqvist, J. Cryst. Growth **59**, 399 (1982).
[27]K. Kukli, M. Ritala, and M. Leskelä, Appl. Phys. Lett. **68**, 3737 (1996).
[28]R. Matero, M. Ritala, M. Leskelä, T. Salo, J. Aromaa, and O. Forssen, J. Phys. IV **9**, Pr8-493 (1999).
[29]E. Härkönen *et al.*, J. Electrochem. Soc. **158**, C369 (2011).
[30]J. Skarp, U.S. patent 4,486,487 (4 December 1984).
[31]K. Kukli *et al.*, ECS J. Solid State Sci. Technol. **7**, P287 (2018).
[32]G. S. Higashi and C. G. Fleming, Appl. Phys. Lett. **55**, 1963 (1989).
[33]J. Ihanus, T. Hatanpää, T. Hänninen, M. Ritala, and M. Leskelä, J. Electrochem. Soc. **151**, H221 (2004).
[34]L. Hiltunen, H. Kattelus, M. Leskelä, M. Mäkelä, L. Niinistö, E. Nykänen, P. Soininen, and M. Tiitta, Mater. Chem. Phys. **28**, 379 (1991).
[35]M. Ritala, K. Kukli, A. Rahtu, P. I. Räisänen, M. Leskelä, T. Sajavaara, and J. Keinonen, Science **288**, 319 (2000).
[36]H. Onishi, N. Sakuma, K. Ieyasu, and Y. Hamakawa, J. Electrochem. Soc. **130**, 2115 (1983).
[37]H. Kobayashi, S. Tanaka, V. Shanker, M. Shiiki, and H. Deguchi, J. Cryst. Growth **72**, 559 (1985).
[38]B. Hüttl, U. Troppenz, K. O. Velthaus, C. R. Ronda, and R. H. Mauch, J. Appl. Phys. **78**, 7282 (1995).
[39]A. Mikami *et al.*, J. Cryst. Growth **110**, 381 (1991).
[40]M. Tammenmaa, T. Koskinen, L. Hiltunen, M. Leskelä, and L. Niinistö, Thin Solid Films **124**, 125 (1985).
[41]A. Hunter and A. H. Kitai, J. Cryst. Growth **91**, 111 (1988).
[42]E. Soininen, G. Härkönen, and K. Vasama, SID Int. Symp. Digest Techn. Papers Suppl. **1**, 77 (2000).
[43]E.L. Soininen, G. Härkönen, M. Lahonen, R. Törnqvist and J. Viljanen U.S. Patent 6,113,977 (5 September 2000).
[44]V. Miikkulainen, M. Ritala, M. Leskelä, and R. L. Puurunen, J. Appl. Phys. **113**, 021301 (2013).
[45]J. A. Lahtinen, A. Lu, T. Tuomi, and M. Tammenmaa, J. Appl. Phys. **58**, 1851 (1985).
[46]M. Oikkonen, M. Tammenmaa, and M. Asplund, Mater. Res. Bull. **23**, 133 (1988).

[47]L. Hiltunen, M. Leskelä, M. Mäkelä, and L. Niinistö, Acta Chem. Scand. Ser. A **41**, 548 (1987).
[48]A. Mikami, K. Terada, K. Okibayashi, K. Tanaka, M. Yoshida, and S. Nakajima, J. Cryst. Growth **110**, 381 (1991).
[49]T. Sutela, Displays **5**, 73 (1984).
[50]A. Ono, *Electroluminescent Displays* (World Scientific, Singapore, 1995).
[51]P. F. Smet, I. Moreels, Z. Hens, and D. Poelman, Materials **3**, 2834 (2010).
[52]D. Theis, H. Oppolzer, G. Eppinghaus, and S. Schild, J. Cryst. Growth **63**, 47 (1983).
[53]J. Benoit, C. Barthou, and P. Benalloul, J. Appl. Phys. **73**, 1435 (1993).
[54]A. Mikami, K. Terada, K. Okibayashi, K. Tanaka, M. Yoshida, and S. Nakajima, J. Appl. Phys. **72**, 773 (1992).
[55]M. Leskelä and L. Niinistö, Mater. Chem. Phys. **31**, 7 (1992).
[56]R. T. Tuenge and J. Kane, SID Digest **22**, 279 (1991).
[57]H. Ohnishi, Ann. Rev. Mater. Sci. **19**, 83 (1989).
[58]H. Yoshino, M. Ohura, S. Kurokawa, and H. Ohnishi, Jpn. Display **92**, 737 (1992).
[59]M. Tammenmaa, M. Leskelä, T. Koskinen, and L. Niinistö, J. Less Common Met. **126**, 209 (1986).
[60]Y. Charreire, A. Marbeuf, G. Tourillon, M. Leskelä, L. Niinistö, E. Nykänen, P. Soininen, and O. Tolonen, J. Electrochem. Soc. **139**, 620 (1992).
[61]M. Leskelä, H. Mölsä, and L. Niinistö, Supercond. Sci. Technol. **6**, 627 (1993).
[62]M. Leskelä, K. Kukli, and L. Niinistö, J. Alloys Compd. **418**, 27 (2006).
[63]J. Ihanus, T. Hänninen, T. Hatanpää, T. Aaltonen, I. Mutikainen, T. Sajavaara, J. Keinonen, M. Ritala, and M. Leskelä, Chem. Mater. **14**, 1937 (2002).
[64]W. A. Barrow, R. E. Coovert, and C. N. King, SID 1984 Digest **15**, 249 (1984).
[65]M. Leppänen, M. Leskelä, L. Niinistö, E. Nykänen, P. Soininen, and M. Tiitta, SID 91 Digest **22**, 282 (1991).
[66]M. Leskelä, J. Alloys Compd. **275–277**, 702 (1998).
[67]Y. Inoue, K. Tanaka, S. Okamoto, K. Kobayashi, and K. Takizawa, Jpn. J. Appl. Phys. **36**, 4335 (1997).
[68]P. D. Rack and P. H. Holloway, Mater. Sci. Eng. R **21**, 171 (1998).
[69]J. Ihanus, E. Lambers, P. H. Holloway, M. Ritala, and M. Leskelä, J. Cryst. Growth **260**, 440 (2004).
[70]D. Poelman, R. Vercaemst, R. L. van Meirhaeghe, W. H. Laflere, and F. Cardon, J. Lumin. **65**, 7 (1995).
[71]T. A. Oberacker and H. W. Schock, J. Cryst. Growth **159**, 935 (1996).
[72]S.-S. Sun, Displays **19**, 145 (1999).
[73]E. Nykänen, S. Lehto, M. Leskelä, L. Niinistö and P. Soininen, *Proceedings of the 6th International Workshop on Electroluminescence*, El-Paso, TX, 11–13 May 1992 (Cinco Puntos, El-Paso, TX, 1992), p. 199.
[74]S. J. Yun, Y. S. Kim, J. S. Kang, S.-H. K. Park, K. I. Cho, and D. S. Ma, SID 1999 Digest **30**, 1142 (1999).
[75]C. N. King, J. SID **4**, 153 (1996).
[76]K. Swiatek, M. Godlewski, L. Niinistö, and M. Leskelä, J. Appl. Phys. **74**, 3442 (1993).
[77]M. Ahonen, M. Pessa, and T. Suntola, Thin Solid Films **65**, 301 (1980).
[78]M. Pessa, R. Mäkelä, and T. Suntola, Appl. Phys. Lett. **38**, 131 (1981).
[79]M. Pessa, P. Huttunen, and M. A. Herman, J. Appl. Phys. **54**, 6047 (1983).
[80]M. Pessa and O. Jylhä, Appl. Phys. Lett. **45**, 646 (1984).
[81]C. H. L. Goodman and M. Pessa, J. Appl. Phys. **60**, R65 (1986).
[82]T. Yao, *Atomic Layer Epitaxy*, edited by T. Suntola and M. Simpson (Blackie, Glasgow, 1990), p. 155.
[83]S. Dosho, Y. Takeura, M. Konagai, and K. Takahashi, Appl. Phys. Lett. **50**, 1686 (1987).
[84]W. Faschinger, F. Hauzenberger, P. Juza, A. Pesek, and H. Sitter, J. Electron Mater. **22**, 497 (1993).
[85]P. Juza, H. Zajicek, H. Sitter, M. Helm, W. Faschinger, and K. Liscka, Appl. Phys. Lett. **61**, 3133 (1992).
[86]C. T. Hsu, Thin Solid Films **335**, 284 (1998).
[87]I. Hernandez-Calderon, J. C. Salcedo-Reyes, A. Alfaro-Martınez, and M. Garcıa-Rocha, Microelectron. J. **36**, 985 (2005).
[88]M.A. Tischler and S.M. Bedair, *Atomic Layer Epitaxy*, edited by T. Suntola and M. Simpson (Blackie, Glasgow, 1990), p. 110.
[89]A. Usui and H. Watanabe, Annu. Rev. Mater. Sci. **21**, 185 (1991).
[90]J. M. Heitzinger, J. M. White, and J. G. Ekerdt, Surf. Sci **299/300**, 892 (1994).
[91]M. A. Tischler and S. M. Bedair, Appl. Phys.Lett. **47**, 51 (1985).
[92]J. Nishizawa, T. Kurabayashi, H. Abe, and A. Nozoe, Surf. Sci. **185**, 249 (1987).
[93]A. Usui and S. Sunakawa, Jpn. J. Appl. Phys. **25**, L212 (1986).
[94]N. Karam, H. Liu, I. Yoshida, N. El-Masry, and S. M. Bedair, Appl. Phys. Lett. **52**, 1144 (1988).
[95]J. Nishizawa, H. Abe, T. Kurabayashi, and N. Sakurai, J. Vac. Sci. Technol. A **4**, 706 (1986).
[96]A. Doi, Y. Aoyagi, and S. Namba, Appl. Phys. Lett. **49**, 785 (1988).
[97]Y. Aoyagi, T. Meguro, S. Iwai, and A. Doi, Mater. Sci. Eng. B **10**, 121 (1991).
[98]J. R. Gong, D. Jung, N. A. El-Masry, and S. M. Bedair, Appl. Phys. Lett. **57**, 400 (1990).
[99]M. Ozeki, Mater. Sci. Rep. **8**, 97 (1992).
[100]W. G. Jeong, E. P. Menu, and D. P. Dapkus, Appl. Phys. Lett. **55**, 244 (1989).
[101]M. Ozeki, K. Kodama, Y. Sakuma, N. Ohtsuka, and T. Takanohashi, J. Vac. Sci. Technol. B **8**, 741 (1990).
[102]D. W. Shaw, J. Electrochem. Soc. **115**, 405 (1986).
[103]S. M. Bedair, B. T. McDermott, Y. Ide, N. H. Karam, H. Hashemi, M. A. Tischler, M. Timmons, J. C. L. Tarn, and N. A. El-Masry, J. Cryst. Growth **93**, 182 (1988).
[104]H. Isshiki, Y. Aoyagi, T. Sugano, S. Iwai, and T. Meguro, Appl. Phys. Lett. **63**, 1528 (1993).
[105]T. Ohno and Y. Oyama, Sci. Technol. Adv. Mater. **13**, 013002 (2012).
[106]C. Ozkit-Akgun, E. Goldenberg, A. K. Okyay, and N. Biyikli, J. Mater. Chem. C **2**, 2123 (2014).
[107]M. Bosund *et al.*, Appl. Surf. Sci. **257**, 7827 (2011).
[108]A. P. Perros, H. Hakola, T. Sajavaara, T. Huhtio, and H. Lipsanen, J. Phys. D Appl. Phys. **46**, 505502 (2013).
[109]P. Motamedi and K. Cadien, Appl. Surf. Sci. **315**, 104 (2014).
[110]S. Bolat, C. Ozkit-Akgun, B. Tekcan, N. Biyikli, and A. Okyay, Appl. Phys. Lett. **104**, 243505 (2014).
[111]B. Tekcan, C. Ozkit-Akgun, S. Bolat, N. Biyikli, and A. Okyay, Opt. Eng. **53**, 107106 (2014).
[112]N. Nepal, N. A. Mahadik, L. O. Nyakiti, S. B. Qadri, M. J. Mehl, J. K. Hite, and C. R. Eddy, Jr., Cryst. Growth Des. **13**, 1485 (2013).
[113]N. Nepal, V. R. Anderson, J. K. Hite, and C. R. Eddy, Jr., Thin Solid Films **589**, 47 (2015).
[114]J. Hite, N. Nepal, V. R. Anderson, J. A. Freitas, M. A. Mastro, and C. R. Eddy, Jr., Proc. SPIE **9755**, 97551W (2016).
[115]J. R. Bakke, K. L. Pickrahn, T. B. Brennan, and S. F. Bent, Nanoscale **3**, 3482 (2011).
[116]A. F. Palmstrom, P. K. Santra, and S. F. Bent, Nanoscale **7**, 12266 (2015).
[117]W. Niu, X. Li, S. K. Karuturi, D. W. Fam, H. Fan, S. Shrestha, L. H. Wong, and A. L. Y. Tok, Nanotechnology **26**, 064011 (2015).
[118]X. Meng, X. Wang, D. Geng, C. Ozgit-Akgun, N. Schneider, and J. W. Elam, Mater. Horizons **4**, 133 (2017).
[119]T. Suntola, MRS Bull. **18**, 45 (1993).
[120]J. Skarp, E. Anttila, A. Rautiainen, and T. Suntola, Int. J. Solar Energy **12**, 137 (1992).
[121]V. Lujala, J. Skarp, M. Tammenmaa, and T. Suntola, Appl. Surf. Sci. **82–83**, 34 (1994).
[122]T. Asikainen, M. Ritala, and M. Leskelä, J. Electrochem. Soc. **141**, 3210 (1994).
[123]T. Asikainen, M. Ritala, and M. Leskelä, J. Electrochem. Soc. **142**, 3538 (1995).
[124]T. Asikainen, M. Ritala, and M. Leskelä, Appl. Surf. Sci. **82–83**, 122 (1994).
[125]T. Tynell and M. Karppinen, Semicond. Sci. Technol. **29**, 043001 (2014).
[126]A. Illiberi, F. Roozeboom, and P. Poodt, ACS Appl. Mater. Interf. **4**, 268 (2012).
[127]C. R. Ellinger and S. F. Nelson, Chem. Mater. **26**, 1514 (2014).
[128]P. Sinsermsuksakul, J. Heo, W. Noh, A. S. Hock, and R. G. Gordon, Adv. Energy Mater. **4**, 140096 (2014).
[129]E. B. Yousfi, T. Asikainen, V. Pietu, P. Cowache, M. Powalla, and D. Lincot, Thin Solid Films **361–362**, 183 (2000).
[130]S. Spiering, D. Hariskos, M. Powalla, N. Naghavi, and D. Lincot, Thin Solid Films **431–432**, 359 (2003).
[131]D. Hariskos, M. Ruckh, U. Ruhle, T. Walter, H. W. Schock, J. Hedstrom, and L. Stolt, Thin Solid Films **480**, 99 (2005).

[132]M. A. Mughal, R. Engelken, and R. Sharma, Solar Energy **120**, 131 (2015).
[133]D. Munoz-Rojas and J. MacManus-Driscoll, Mater. Horizons **1**, 314 (2014).
[134]J. Lindahl, J.T. Wätjen, A. Hultqvist, T. Ericson, M. Edoff, and T. Törndahl, Prog. Photovolt. Res. Appl. **21**, 1588 (2013).
[135]J. Löckinger *et al.*, ACS Appl. Mater. Interf. **10**, 43603 (2018).
[136]G. Agostinelli, A. Delabie, P. Vitanov, Z. Alexieva, H. F. W. Dekkers, S. De Wolf, and G. Beaucarne, Solar Energy Mater. Solar Cells **90**, 3438 (2006).
[137]J. Benick, B. Hoex, M. C. M. van de Sanden, W. M. M. Kessels, O. Schultz, and S. W. Glunz, Appl. Phys. Lett. **92**, 253504 (2008).
[138]B. Hoex, J. Schmidt, R. Bock, P. P. Altermatt, M. C. M. van de Sanden, and W. M. M. Kessels, Appl. Phys. Lett. **91**, 112107 (2007).
[139]B. Hoex, J. J. H. Gielis, M. C. M. van de Sanden, and W. M. M. Kessels, J. Appl. Phys. **104**, 113703 (2008).
[140]G. Dingemans and W. M. M. Kessels, J. Vac. Sci. Technol. A **30**, 040802 (2012).
[141]G. Dingemans, M. C. M. van de Sanden, and W. M. M. Kessels, Phys. Status Solidi RRL **5**, 22 (2011).
[142]H. Savin, P. Repo, G. von Gastrow, P. Ortega, E. Calle, M. Garin, and R. Alcubilla, Nat. Nanotech. **10**, 624 (2015).
[143]D. H. Levy, D. Freeman, S. F. Nelson, P. J. Cowdery-Corvan, and L. M. Irving, Appl. Phys. Lett. **92**, 192101 (2008).
[144]B. Vermang, A. Rothschild, A. Racz, J. John, J. Poortmans, R. Mertens, P. Poodt, V. Tiba, and F. Roozeboom, Prog. Photovolt. Res. Appl. **19**, 733 (2011).
[145]S. Yin, A. Riapanitra, and Y. Asakura, Funct. Mater. Lett. **11**, 1830004 (2018).
[146]A. Listorti, B. O'Reagan, and J. R. Durrant, Chem. Mater. **22**, 3381 (2011).
[147]M. Law, L. E. Greene, A. Radenovic, T. Kuykendall, J. Liphardt, and P. Yang, J. Phys. Chem. B **110**, 22652 (2006).
[148]L. J. Antila *et al.*, J. Phys.Chem. C **133**, 16720 (2011).
[149]L. J. Antila, M. J. Heikkilä, V. Aumanen, M. Kemell, P. Myllyperkiö, M. Leskelä, and J. Korppi-Tommola, J. Phys. Chem. Lett. **1**, 536 (2010).
[150]E. Palomares, J. N. Clifford, S. A. Haque, T. Lutz, and J. R. Durrant, J. Am. Chem. Soc. **125**, 475 (2003).
[151]C. Lin, F. Tsai, M. Lee, C. Lee, T. Tien, L. Wang, and S. Tsai, J. Mater. Chem. **19**, 2999 (2009).
[152]A. K. Chandiran, M. K. Nazeeruddin, and M. Grätzel, Adv. Funct. Mater. **24**, 1615 (2014).
[153]A. K. Chandiran, N. Tetreault, R. Humphry-Baker, F. Kessler, E. Baranoff, C. Yi, M. K. Nazeeruddin, and M. Grätzel, Nano Lett. **12**, 3941 (2012).
[154]T. W. Hamann, A. B. F. Martinson, J. W. Elam, M. J. Pellin, and J. T. Hupp, J. Phys. Chem. C **112**, 10303 (2008).
[155]A. K. Chandiran, P. Comte, R. Humphry-Baker, F. Kessler, C. Yi, M. K. Nazeeruddin, and M. Grätzel, Adv. Funct. Mater. **23**, 2775 (2013).
[156]H. Wang, Z. Guo, S. Wang, and W. Liu, Thin Solid Films **558**, 1 (2014).
[157]A. B. F. Martinson, T. W. Hamann, M. J. Pellin, and J. T. Hupp, Chem. Eur. J. **14**, 4458 (2008).
[158]Q. Zhang, C. S. Dandeneau, X. Zhou, and C. Cao, Adv. Mater. **21**, 4087 (2009).
[159]A. B. F. Martinson, J. W. Elam, J. T. Hupp, and M. J. Pellin, Nano Lett. **7**, 2183 (2007).
[160]L. Loh and S. Dunn, J. Nanosci. Nanotechnol. **12**, 8215 (2012).
[161]A. K. Chandiran, M. Abdi-Jalebi, M. K. Nazeeruddin, and M. Grätzel, ACS Nano **8**, 2261 (2014).
[162]J.-H. Yum, T. Moehl, J. Yoon, A. K. Chandiran, F. Kessler, P. Gratia, and M. Grätzel, J. Phys. Chem. C **118**, 16799 (2014).
[163]R. L. Z. Hoye, K. P. Musselman, and J. L. MacManus-Driscoll, APL Mater. **1**, 060701 (2013).
[164]M. Grätzel and N.-G. Park, Nano **9**, 1440002 (2014).
[165]M. Grätzel, Nature Mater. **13**, 838 (2014).
[166]W. S. Yang *et al.*, Science **356**, 1376 (2017).
[167]A. K. Chandiran, A. Yella, M. T. Mayer, P. Gao, M. K. Nazeeruddin, and M. Grätzel, Adv. Mater. **26**, 4309 (2014).
[168]C.-Y. Chang, K.-T. Lee, W.-K. Huang, H.-Y. Siao, and Y.-C. Chang, Mater. Chem. **27**, 5122 (2015).
[169]H. Liu, Z. Huang, S. Wei, L. Zheng, L. Xioa, and Q. Gong, Nanoscale **8**, 6209 (2016).
[170]V. Zardetto, B. L. Williams, A. Perrotta, F. Di Giacomo, M. A. Verheijen, R. Andriessen, W. M. M. Kessels, and M. Creatore, Sust. Energy Fuels **1**, 30 (2017).
[171]H. Wei *et al.*, Phys.Chem. Chem. Phys. **17**, 4937 (2015).
[172]B. R. Sutherland *et al.*, Adv. Mater. **27**, 53 (2015).
[173]G. Popov, M. Mattinen, T. Hatanpää, M. Vehkamäki, M. L. Kemell, K. Mizohata, J. Räisänen, M. Ritala, and M. Leskelä, Chem. Mater. **31**, 1101 (2019).
[174]B. J. Kim *et al.*, Energy Environ. Sci. **8**, 916 (2015).
[175]B. Radisavljevic, A. Radenovic, J. Brivio, V. Giacometti, and A. Kis, Nat. Nanotechnol. **6**, 147 (2011).
[176]M. Samadi, N. Sarikhani, M. Zirak, H. Zhang, H.-L. Zhang, and A. Z. Moshfegh, Nanoscale Horizons **3**, 90 (2018).
[177]C. Yan *et al.*, Adv. Funct. Mater. **28**, 1803305 (2018).
[178]M. Rahman, K. Davey, and S.-Z. Qiao, Adv. Funct. Mater. **27**, 1606129 (2017).
[179]G. H. Han, D. L. Duong, D. H. Keum, S. J. Yun, and Y. H. Lee, Chem. Rev. **118**, 6297 (2018).
[180]K. F. Mak and J. Shan, Nat. Photonics **10**, 216 (2016).
[181]C. Xie, C. Mak, X. Tao, and F. Yan, Adv. Funct. Mater. **27**, 1603886 (2017).
[182]S. Das, D. Pandey, J. Thomas, and T. Roy, Adv. Mater. **31**, 1802722 (2019).
[183]L. Liu, H. Yao, H. Li, Z. Wang, and Y. Shi, FlatChem **10**, 22 (2018).
[184]J. Wang, I. Verzhbitskiy, and G. Eda, Adv. Mater. **30**, 1802687 (2018).
[185]Y. P. V. Subbaiah, K. J. Saji, and A. Tiwari, Adv. Funct. Mater. **26**, 2046 (2016).
[186]T. A. Ho, C. Bae, S. Lee, M. Kim, J. M. Montero-Moreno, J. H. Park, and H. Shin, Chem. Mater. **29**, 7604 (2017).
[187]L. K. Tan, B. Liu, J. H. Teng, S. Guo, H. Y. Low, and K. P. Loh, Nanoscale **6**, 10584 (2014).
[188]R. Browning, P. Padigi, R. Solanki, D. J. Tweet, P. Schuele, and D. Evans, Mater. Res. Express **2**, 035006 (2015).
[189]Y. Huang, L. Liu, J. Sha, and Y. Chen, Appl. Phys. Lett. **111**, 063902 (2017).
[190]L. Liu, Y. Huang, J. Sha, and Y. Chen, Nanotechnology **28**, 195605 (2017).
[191]Y. Kim *et al.*, Sci. Rep. **6**, 18754 (2016).
[192]M. B. Sreedhara, S. Gope, B. Vishal, R. Datta, A. J. Bhattacharyya, and C. N. R. Rao, J. Mater. Chem. A **6**, 2302 (2018).
[193]A. Valdivia, D. J. Tweet, and J. F. Conley, Jr, J. Vac. Sci. Technol. A **34**, 021515 (2016).
[194]Y. Huang, L. Liu, W. Zhao, and Y. Chen, Thin Solid Films **624**, 101 (2017).
[195]Y. Huang, L. Liu, J. Lv, J. Yang, J. Sha, and Y. Chen, AIP Adv. **8**, 045216 (2018).
[196]C. MacIsaac, J. R. Schneider, R. G. Closser, T. R. Hellstern, D. S. Bergsman, J. Park, Y. Liu, R. Sinclair, and S. F. Bent, Adv. Funct. Mater. **28**, 1800852 (2018).
[197]Z. Jin, S. Shin, D. H. Kwon, S.-J. Han, and Y.-S. Min, Nanoscale **6**, 14453 (2014).
[198]J. J. Pyeon, S. H. Kim, D. S. Jeong, S.-H. Baek, C.-Y. Kang, J.-S. Kim, and S. K. Kim, Nanoscale **8**, 10792 (2016).
[199]Y. Jang, S. Yeo, H.-B.-R. Lee, H. Kim, and S.-H. Kim, Appl. Surf. Sci. **365**, 160 (2016).
[200]D. K. Nandi, U. K. Sen, D. Choudhury, S. Mitra, and S. K. Sarkar, Electrochim. Acta **146**, 706 (2014).
[201]D. Xiong, Q. Zhang, W. Li, J. Li, X. Fu, M. F. Cerqueira, P. Alpuim, and L. Liu, Nanoscale **9**, 2711 (2017).
[202]S. Oh, J. B. Kim, J. T. Song, J. Oh, and S.-H. Kim, J. Mater. Chem. A **5**, 3304 (2017).
[203]D. K. Nandi, S. Sahoo, S. Sinha, S. Yeo, H. Kim, R. N. Bulakhe, J. Heo, J.-J. Shim, and S.-H. Kim, ACS Appl. Mater. Interfaces **9**, 40252 (2017).
[204]T. Zhang, Y. Wang, J. Xu, L. Chen, H. Zhu, Q. Sun, S. Ding, and D. W. Zhang, 2D Mater. **5**, 015028 (2018).
[205]S. Shin, Z. Jin, D. H. Kwon, R. Bose, and Y.-S. Min, Langmuir **31**, 1196 (2015).
[206]X. Li, M. Puttaswamy, Z. Wang, C. K. Tan, A. C. Grimsdale, N. P. Kherani, and A. I. Y. Tok, Appl. Surf. Sci. **422**, 536 (2017).
[207]D. H. Kwon, Z. Jin, S. Shin, W.-S. Lee, and Y.-S. Min, Nanoscale **8**, 7180 (2016).
[208]W. Jeon, Y. Cho, S. Jo, J.-H. Ahn, and S.-J. Jeong, Adv. Mater. **29**, 1703031 (2017).

[209]J. Kuhs, T. Dobbalaere, Z. Hens, and C. Detavernier, J. Vac. Sci. Technol. A **35**, 01B111 (2017).
[210]K. Ellmer and D. Lichtenberger, Surf. Coat. Technol. **74–75**, 586 (1995).
[211]S. Cadot *et al.*, Nanoscale **9**, 538 (2017).
[212]A. U. Mane, S. Letourneau, D. J. Mandia, J. A. Libera, Y. Lei, Q. Peng, E. Graugnard, and J. W. Elam, J. Vac. Sci. Technol. A **36**, 01A125 (2018).
[213]S. Letourneau, M. J. Young, N. M. Bedford, Y. Ren, A. Yanguas-Gil, A. U. Mane, J. W. Elam, and E. Graugnard, ACS Appl. Nano Mater. **1**, 4028 (2018).
[214]A. Sharma *et al.*, Nanoscale **10**, 8615 (2018).
[215]T. Jurca, M. J. Moody, A. Henning, J. D. Emery, B. Wang, J. M. Tan, T. L. Lohr, L. J. Lauhon, and T. J. Marks, Angew. Chem. Int. Ed. **56**, 4991 (2017).
[216]V. Pore, T. Hatanpää, M. Ritala, and M. Leskelä, J. Am. Chem. Soc. **131**, 3478 (2009).
[217]M. Krbal, J. Prikryl, R. Zazpe, F. Dvorak, F. Bures, and J. M. Macak, Phys. Status Solidi Rapid Res. Lett. **12**, 1800023 (2018).
[218]S. Ng *et al.*, Adv. Mater. Interfaces **5**, 1701146 (2018).
[219]J. Hämäläinen, M. Mattinen, K. Mizohata, K. Meinander, M. Vehkamäki, J. Räisänen, M. Ritala, and M. Leskelä, Adv. Mater. **30**, 1703622 (2018).
[220]X. Zhou, Q. Zhang, L. Gan, H. Li, J. Xiong, and T. Zhai, Adv. Sci. **3**, 1600177 (2016).
[221]E. Thimsen, S. C. Riha, S. V. Baryshev, A. B. F. Martinson, J. W. Elam, and M. J. Pellin, Chem. Mater. **24**, 3188 (2012).
[222]E. Thimsen, S. V. Baryshev, A. B. F. Martinson, J. W. Elam, I. V. Veryovkin, and M. J. Pellin, Chem. Mater. **25**, 313 (2013).
[223]C. Hägglund, G. Zeltzer, R. Ruiz, I. Thomann, H.-B.-R. Lee, M. L. Brongersma, and S. F. Bent, Nano Lett. **13**, 3352 (2013).
[224]G. Ham, S. Shin, J. Park, H. Choi, J. Kim, Y.-A. Lee, H. Seo, and H. Jeon, ACS Appl. Mater. Interfaces **5**, 8889 (2013).
[225]W. Seo, S. Shin, G. Ham, J. Lee, S. Lee, H. Choi, and H. Jeon, Jpn. J. Appl. Phys. **56**, 031201 (2017).
[226]G. Ham, S. Shin, J. Park, J. Lee, H. Choi, S. Lee, and H. Jeon, RSC Adv. **6**, 54069 (2016).
[227]S. Lee, S. Shin, G. Ham, J. Lee, H. Choi, H. Park, and H. Jeon, AIP Adv. **7**, 045307 (2017).
[228]J. Lee *et al.*, AIP Adv. **7**, 025311 (2017).
[229]H. Choi *et al.*, Nanotechnology **29**, 215201 (2018).
[230]M. Mattinen, P. J. King, L. Khriachtchev, K. Meinander, J. T. Gibbon, V. R. Dhanak, J. Räisänen, M. Ritala, and M. Leskelä, Small **14**, 1800547 (2018).
[231]J. Schmitz, Surf. Coat. Technol. **343**, 83 (2018).
[232]V. Pore, M. Ritala, and M. Leskelä, Chem. Vap. Deposition **13**, 163 (2007).
[233]N. Mahuli and S. K. Sarkar, J. Vac. Sci. Technol. A **33**, 01A150 (2015).
[234]T. W. Scharf, S. V. Prasad, M. T. Dugger, P. G. Kotula, R. S. Goeke, and R. K. Grubbs, Acta Mater. **54**, 4731 (2006).
[235]T. W. Scharf, D. R. Diercks, B. P. Gorman, S. V. Prasad, and M. T. Dugger, Tribol. Trans. **52**, 284 (2009).
[236]A. Delabie *et al.*, Chem. Commun. **51**, 15692 (2015).
[237]B. Groven *et al.*, Chem. Mater. **29**, 2927 (2017).
[238]B. Groven *et al.*, J. Vac. Sci. Technol. A **36**, 01A105 (2018).
[239]B. Groven *et al.*, Chem. Mater. **30**, 7648 (2018).
[240]T. Schram *et al.*, in *Proceedings in 47th European Solid-State Device Research Conference*, Leuven, Belgium, 11–14 September 2017 (IEEE, 2017), pp. 212–215.
[241]R. Browning, P. Plachinda, P. Padigi, R. Solanki, and S. Rouvimov, Nanoscale **8**, 2143 (2015).
[242]D. K. Nandi, U. K. Sen, A. Dhara, S. Mitra, and S. K. Sarkar, RSC Adv. **6**, 38024 (2016).
[243]Y. Sun, Z. Chai, X. Lu, and J. Lu, Tribol. Int. **114**, 478 (2017).
[244]Y. Sun, Z. Chai, X. Lu, and D. He, Sci. China Technol. Ser. **60**, 51 (2016).
[245]S. Yeo *et al.*, Appl. Surf. Sci. **459**, 596 (2018).
[246]A. Eftekhari, J. Mater. Chem. A **5**, 18299 (2017).
[247]Y.-C. Lin *et al.*, ACS Nano **12**, 965 (2018).
[248]K. Park, Y. Kim, J.-G. Song, S. J. Kim, C. W. Lee, G. H. Ryu, Z. Lee, J. Park, and H. Kim, 2D Mater. **3**, 014004 (2016).
[249]R. Browning, N. Kuperman, R. Solanki, V. Kanzyuba, and S. Rouvimov, Semicond. Sci. Technol. **31**, 095002 (2016).
[250]K. Y. Ko, K. Park, S. Lee, Y. Kim, W. J. Woo, D. Kim, J.-G. Song, J. Park, and H. Kim, ACS Appl. Mater. Interfaces **10**, 23910 (2018).
[251]T. W. Scharf, S. V. Prasad, T. M. Mayer, R. S. Goeke, and M. T. Dugger, J. Mater. Res. **19**, 3443 (2004).
[252]M. Bernardi, M. Palummo, and J. C. Grossman, Nano Lett. **13**, 3664 (2013).
[253]A. U. Rehman *et al.*, ACS Appl. Mater. Interfaces **8**, 29383 (2016).